Geologica Acta, Vol.11, Nº 1, March 2013, 1-26
DOI: 10.1344/105.000001780
Available online at www.geologica-acta.com

geologica acta

Structural evolution of Pico del Águila anticline (External Sierras, southern Pyrenees) derived from sandbox, numerical and 3D structural modelling techniques

O. VIDAL-ROYO [1] **J.A. MUÑOZ** [1] **S. HARDY** [1,2] **H.KOYI** [3] **N.CARDOZO** [4]

[1] **Geomodels Research Centre. GGAC, Departament de Geodinàmica i Geofísica, Facultat de Geologia**
Universitat de Barcelona (UB)
C/ Martí i Franquès s/n, 08028, Barcelona, Spain

[2] **Institució Catalana de Recerca i Estudis Avançats (ICREA)**
Catalonia, Spain

[3] **Hans Ramberg Tectonic Laboratory, Department of Earth Sciences, Uppsala University**
Villavägen 16, SE-752 36, Uppsala, Sweden

[4] **Department of Petroleum Engineering, University of Stavanger**
4036 Stavanger, Norway

ABSTRACT

This paper reports on the integration of different modelling techniques to construct a unified conceptual model of structural evolution of the Pico del Águila anticline (External Sierras, southern Pyrenees, Spain). The structure is a well-known example of a detachment fold, which exhibits a N-S structural trend, perpendicular to the general structural trend of the southern Pyrenees (mainly E-W). Based on field observations of an unevenly distributed Triassic décollement, analogue modelling shows how to generate orogen-perpendicular structures which may result in transverse anticlines. The models show how contrasts between high and low friction patches in the basal décollement led to the formation of structures at high angle, centered over the high friction areas. Numerical models investigate the effect of a complex mechanical stratigraphy, characterized by an interlayering of competent and incompetent layers, plus syn-kinematic sedimentation in the fold growth. Based on field data and seismic interpretations, a 3D reconstruction and sequential geomechanical restoration of the Pico del Águila anticline suggests the coexistence of multiple folding mechanisms occurring simultaneously in different units and structural domains of the fold, leading to a complex strain pattern that can not be assessed by simplistic kinematic 2D approaches. By integrating the models with previous data in the region, the benefits and drawbacks of each modelling technique are discussed and an integrated model of structural evolution for the Pico del Águila anticline is presented. This enables a better comprehension of the structure as well as of the processes that drove the evolution of the N-S detachment anticlines in the External Sierras of the southern Pyrenees.

KEYWORDS | **Analogue modelling. Numerical modelling. 3D reconstruction. Geomechanical restoration. Detachment anticline. Pico del Águila. External Sierras.**

INTRODUCTION

The Pico del Águila anticline (External Sierras, southern Pyrenees, Spain) is one of the most renowned examples of transverse detachment folding with marine to fluvio-deltaic associated sedimentation. The anticline is characterized by a N-S structural trend, exhibiting an interesting interference pattern with the perpendicular E-W trend of the Pyrenean orogen. In the lack of any E-W directed tectonic event (Pueyo *et al*., 2002; Huyghe *et al*., 2009, Vidal-Royo *et al*., 2009), the origin and evolution of the Pico del Águila anticline has remained a matter of study for many geoscientists from all over the world and has been studied by many different disciplines in the Earth Sciences. Its well preserved, easily accessible sedimentary record of the growth strata purveys a good control on the evolution of the fold growth (Poblet and Hardy, 1995; Vidal-Royo *et al*., 2011a), as well as a basis for detailed sedimentological and paleomagnetic analysis (Millán *et al*., 1994; Pueyo *et al*., 2002; Castelltort *et al*., 2003, Rodríguez-Pintó *et al*., 2008). However, the complexity of the structure in 3D, the fold kinematics and the lack of research considering the entire structure in 3D have evidenced the necessity to carry out a study based on the integration of different modelling techniques, in order to produce a better constrained model of the geodynamic evolution of the anticline.

Geological models in Earth Sciences provide explanations and improve the understanding of the geological processes that may take place in the planet. In most cases, they should not purport to be a direct replica of nature but a way to simulate and represent geological processes in a feasible timescale for human-beings.

Structural geology has a long history in the use of modelling as a tool to better understand the generation and evolution of structures. Since the first attempts in sandbox experiments (Hall, 1815; Daudre, 1879; Cadell, 1888; among others), a wide variety of modelling techniques have arisen and developed as a result of geoscientists' needs to solve new concerns. Analogue models have become more sophisticated, incorporating elements and devices that produce more quantitative results to compare with nature (Koyi, 1997). With the rise and spread of computers, numerical models have been developed in contribution with mathematical algorithms that brought great advances in the understanding of geological processes (Krumbein and Graybill, 1965; Agterberg, 1967; Harbaugh and Merriam, 1968). In this sense, numerical models added a quantitative control of the laws and parameters that govern natural processes.

Despite these advances, each modelling technique has particular strengths, weaknesses and limitations, which results in a relatively simplified or incomplete representation of nature. This makes each approach suitable for certain purposes, keeping in mind that knowing the limitations of the technique is essential to correctly understand what a model is purporting to represent. For this reason, behind each model there should be feasible parameters to test and/or observable processes to unveil, rather than an attempt to make a detailed replica of a natural case.

In this study, three different modelling approaches are presented to better understand the structural evolution of the N-S anticlines in the External Sierras of the southern Pyrenees (Northeast Spain). The Pico del Águila anticline is the best-exposed of these structures, being considered a world-class example of a detachment anticline. In addition, the geological map of the anticline can be understood as a down-plunge section. The N-S transverse anticlines are characterized by the interference pattern with the E-W Pyrenean-trend structures. The N-S anticlines show a high degree of preservation of the entire growth strata record, which allows us to constrain the timing of deformation. The structure is well-known and has been described from the points of view of sedimentological analysis (Millán *et al*., 1994; Castelltort *et al*., 2003), paleomagnetism (Pueyo *et al*., 2002; Rodríguez-Pintó *et al*., 2008), analogue modelling (Nalpas *et al*., 1999, 2003), 2D kinematical models (Poblet and Hardy, 1995; Poblet *et al*., 1997), restoration of cross sections (Novoa *et al*., 2000) and other multidisciplinary approaches (Huyghe *et al*., 2009). Despite this, an integrated kinematic understanding of the formation of this range-perpendicular anticline remains unclear.

In our study we first present a 3D reconstruction of the Pico del Águila, from which the geometry of the interference pattern between N-S and E-W structures is unveiled. In addition to providing answers about the structural evolution and the interference pattern between N-S and E-W structures, the 3D model poses new questions about the geological processes that took place in the generation and evolution of the anticline. These questions were tackled by using different modelling techniques, which are presented after the 3D model. In this sense, our study aims to present a unified and better constrained model of structural evolution based on the integration of results from analogue modelling (Vidal-Royo *et al*., 2009), 2D mechanical models (Vidal-Royo *et al*., 2011a) and 3D geomechanical restoration of the Pico del Águila anticline (Vidal-Royo *et al*., 2011b). For this particular case, investigating the structure of the Pico del Águila by means of integrating different approaches has become essential to correctly interpret its evolution. These techniques have helped us: to understand the processes that originated the structure at high angle with the general structural trend and drove its vertical axis rotation; to gain insight on how the mechanical properties of each unit

control the growth of the anticline; to better understand the role of the growth strata, and how these syn-kinematic units have recorded the folding mechanisms that took place and to show how these mechanisms may interact in 3D simultaneously in different units and fold domains, giving rise to a rather complex evolution of the structure when analyzed in three dimensions. The presented analogue models show how orogen-perpendicular structures can be generated in a single event of shortening due to strong mechanical contrasts in the basal décollement level. The numerical models evaluate the importance of mechanical stratigraphy and syn-kinematic sedimentation in the growth of a detachment anticline such as the Pico del Águila. Finally, the 3D geomechanical restoration shows the complexity of the interference pattern in the Pico del Águila anticline, its sequential evolution through time as well as the combination of multiple folding mechanisms acting simultaneously during the fold growth.

GEOLOGICAL SETTING

The geology of the External Sierras is widely known and reported in many studies through the years. The interested reader will find accurate descriptions of the field geology in key publications as Puigdefàbregas (1975), Millán *et al.* (1994), and Pueyo *et al.* (2002). However, a general overview is offered for the reader to better understand the content of the manuscript.

The Pico del Águila anticline is located in the External Sierras ("Sierras Exteriores Aragonesas") of the southern Pyrenees. The External Sierras consists of several imbricated thrust sheets of primarily Eocene to Oligocene strata detached on evaporitic, calcareous and dolomitic facies of the Middle and Upper Triassic (Muschelkalk and Keuper facies) (Soler and Puigdefàbregas, 1970; IGME, 1992; Millán *et al.* 1994; Millán, 1995; Pueyo *et al.*, 2002). The External Sierras constitutes the frontal emerging part of the South-Pyrenean thrust sheet and is displaced southwards over the Tertiary sediments of the Ebro foreland basin.

As mentioned, one of the peculiarities of the central External Sierras is the presence of a set of N-S to NW-SE anticlines. These structures are perpendicular to the general structural trend of the Pyrenees (E-W; tectonic transport towards the south) and create a complex interference

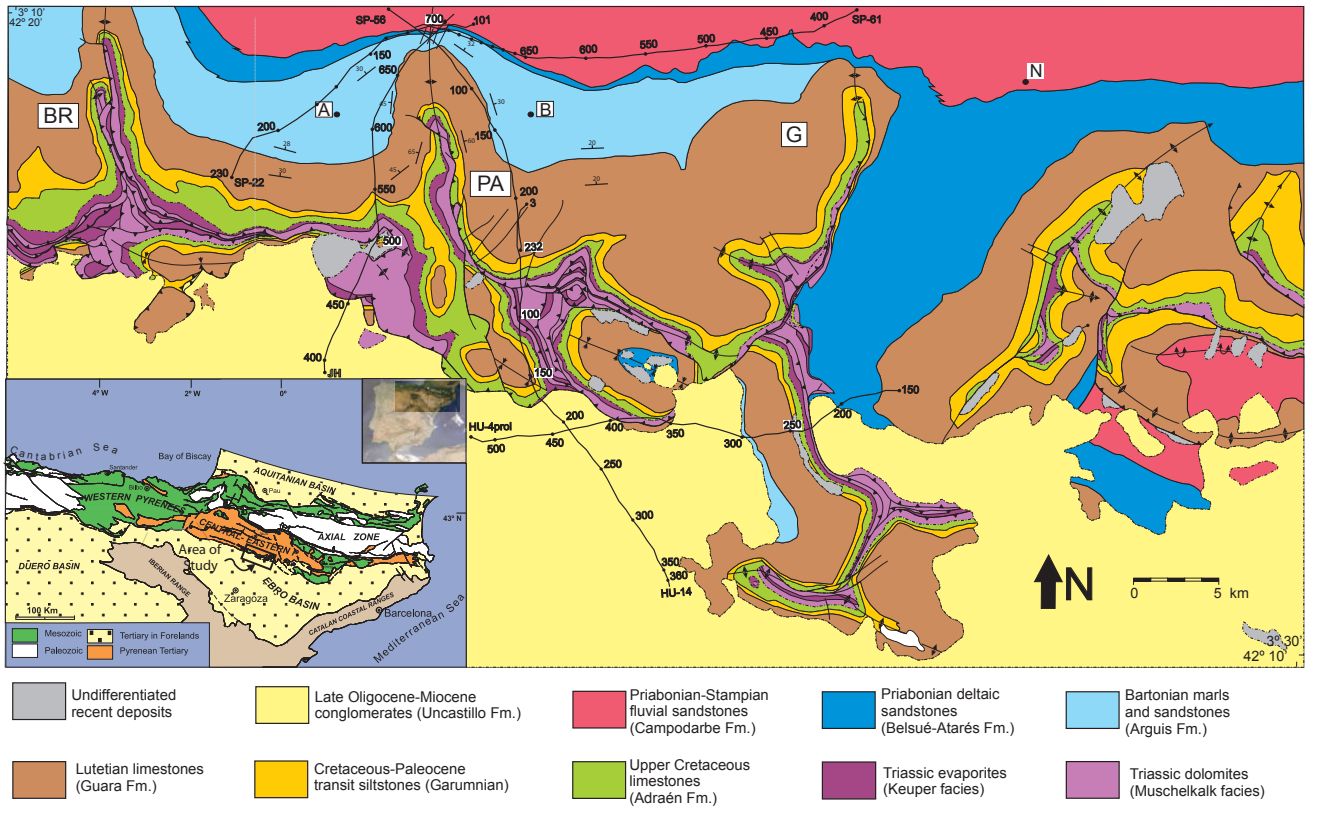

FIGURE 1 | Geological map of the central external Sierras (modified from IGME, 1992). BR: Bentué de Rasal anticline; PA: Pico del Águila anticline; G: Gabardiella anticline complex; A: Arguis Village; B: Belsué village. Inset shows the location and the regional tectonic setting of the study area. Black lines indicate the seismic profiles used to reconstruct the morphology of the Pico del Águila at depth.

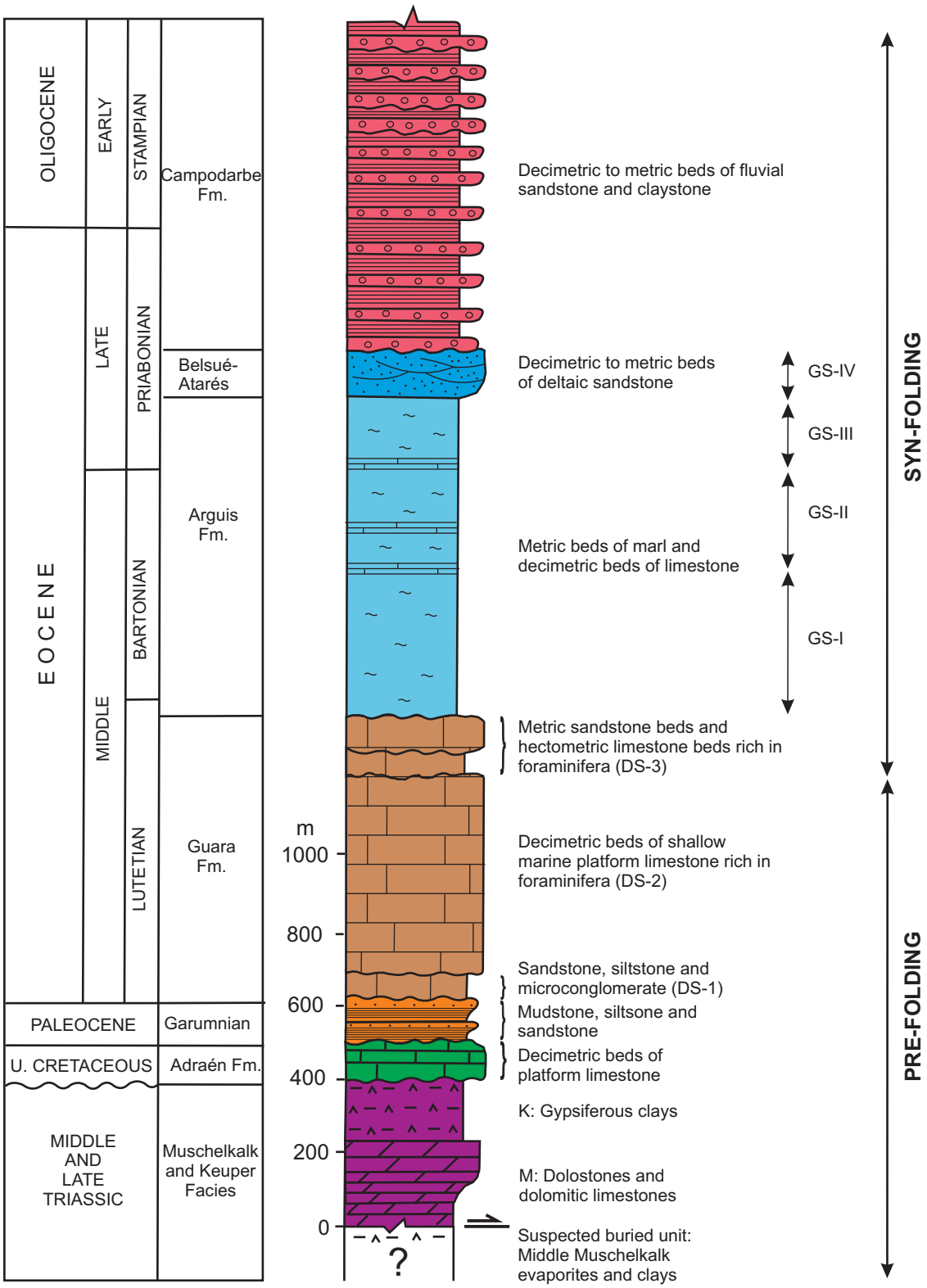

FIGURE 2 | Stratigraphic column describing the lithologies and average thicknesses of the lithologies found in the central External Sierras. M: Muschelkalk facies; K: Keuper facies. DS: Depositional sequences within Guara Fm. GS: Depositional sequences within the growth strata (Arguis and Belsué-Atarés fms.). Modified after Millán *et al.*, 1994.

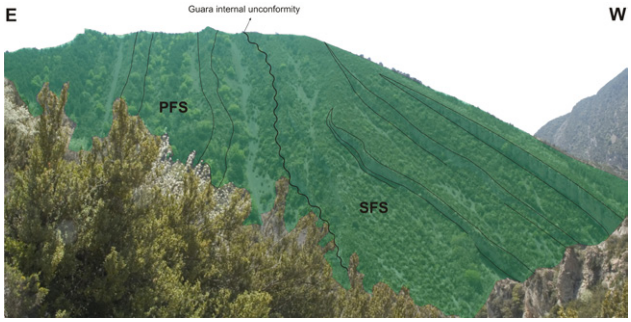

FIGURE 3 | Oblique photograph of the uppermost part of the western limb looking south. It shows an internal unconformity of Guara limestone Fm. that separates the Pre-Folding Sequence (PFS) and the Syn-Folding sequence (SFS). Note how the horizons of the SFS clearly thin towards the E.

pattern (Fig. 1). The N-S anticlines become younger and smaller westwards (Millán *et al.*, 1994; Millán, 1995) and their growth was synchronous with the deposition of middle Eocene to Oligocene sediments (Fig. 2) and the development of the South-Pyrenean thrust front (active until Early Miocene times; Puigdefàbregas, 1975; Holl and Anastasio, 1993; Millán *et al.*, 1994; Millán, 1995).

Timing of the formation of the Pico del Águila anticline is well-constrained by paleomagnetism with growth beginning at 42.67±0.02Ma (upper Lutetian) and finishing at 34.8±1.72Ma (lower Priabonian) (Poblet and Hardy, 1995). The anticline displays a spectacular growth strata record (Figs. 3, 4) (Millán *et al.*, 1994; Millán, 1995; Poblet and Hardy, 1995; Pueyo *et al.*, 2002; Castelltort *et al.*, 2003; Vidal-Royo *et al.*, 2011a).

The stratigraphic record of the central External Sierras is an interlayered sequence of competent and incompetent units (Millán *et al.*, 1994). The stratigraphy of the area consists of a few hundred metres thick Mesozoic succession covered by a thicker Paleogene sequence (Fig. 2). The Mesozoic consists of Triassic limestones, dolomites and gypsum-bearing clays, and Upper Cretaceous shallow marine limestones. The Paleogene comprises continental sandstones, siltstones and lacustrine limestones of the Cretaceous-Paleocene transition (Garumnian facies), shallow marine platform limestones of the Guara

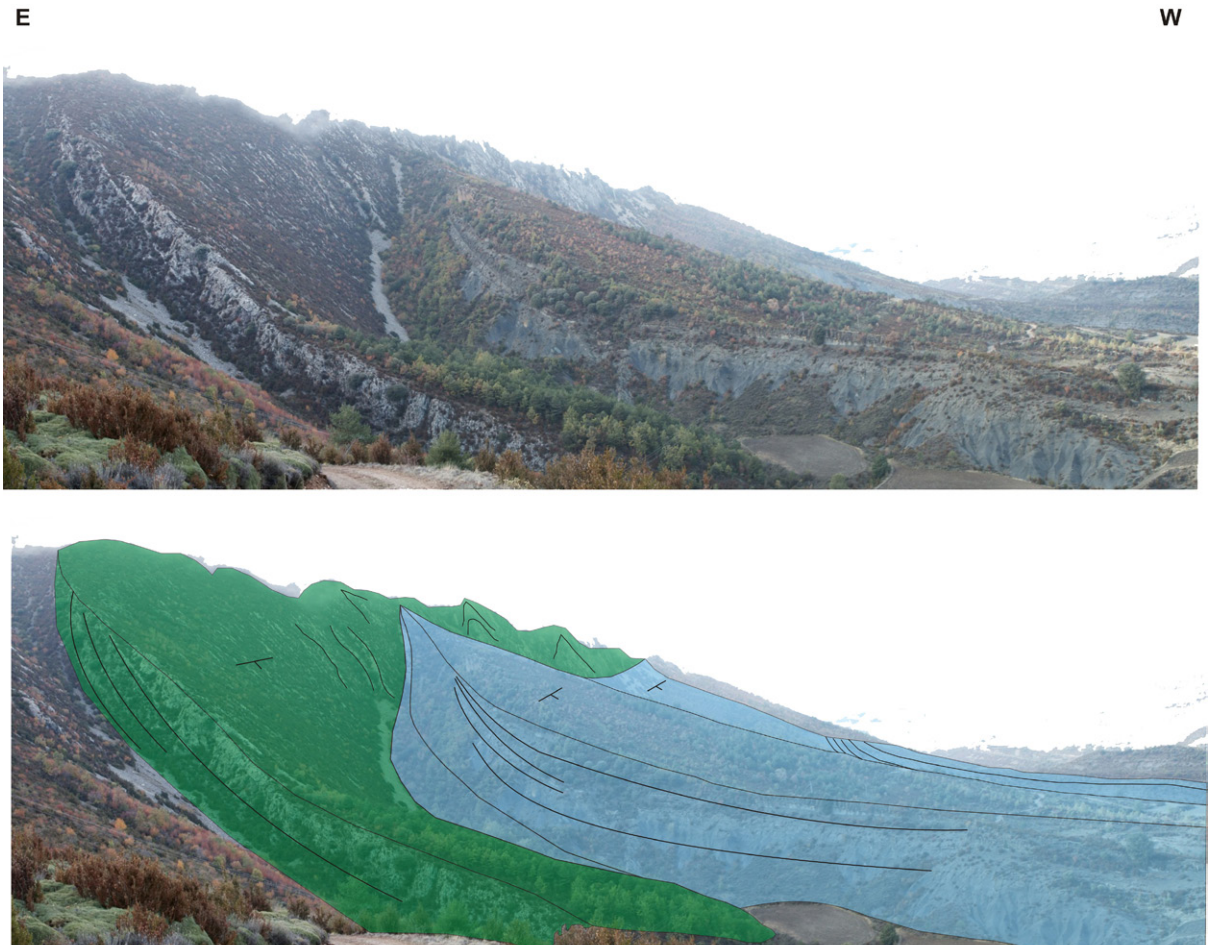

FIGURE 4 | Oblique photograph of the eastern limb of Pico del Águila anticline looking North. One can clearly observe the onlap of Arguis marls (in blue) thinning towards the Guara limestones (in green).

anticlinal (Lutetian), shallow marine and transitional marls, limestones and deltaic sandstones of the Arguis and Belsué-Atarés fms. (upper Lutetian to middle Priabonian), and fluvial clays, sandstones and conglomerates of the Campodarbe Fm. (middle Priabonian to middle Oligocene).

The pre-folding sequence comprises Triassic to Lutetian rocks with the upper limit at the top of the depositional sequence 2 of the Guara Fm. The décollement level is defined by Triassic units. Field observations and geological mapping (IGME, 1992) indicate that Muschelkalk limestones and dolomites (Middle Triassic rocks) are the oldest units outcropping in the core of the anticline (Fig. 1), being internally thrusted, and highly deformed. Keuper clays and evaporites (Upper Triassic rocks) outline the geometry of the fold with an important decrease of thickness observed towards the inner part, where it is nearly absent in the core of the anticline (Fig. 1). In such a way, Keuper facies are thicker and better exposed in the areas between, rather than in the core of the N-S anticlines, where the frontal South-Pyrenean thrust emerges.

The syn-folding sequence comprises the depositional sequence 3 of the Guara Fm. (Fig. 3) and the shallowing upwards (marine to continental) sequence formed by the Arguis, the Belsué-Atarés and the base of the Campodarbe fms. The base of the Arguis Fm. defines a regional unconformity, indicating a rapid change to slope depositional environments (Figs. 2; 4). Millán *et al.* (1994) defined four major depositional sequences within the Arguis and Belsué-Atarés fms. Sequence I (named GS-I herein) is made of late Lutetian to early Bartonian blue marls and sandy glauconite-bearing marls. This sequence thins towards the crest of the anticline and is not existent at the hinge area (Fig. 4). Sequence II (named GS-II herein) is middle to late Bartonian in age, and comprises barely bioturbated blue marls. Sequence III (named GS-III herein) is a platform rich in pectinids of early Priabonian age, formed by barely bioturbated blue marls rich in marine fossil content. Sequence IV (named GS-IV herein) is formed by early Priabonian deltaic sandy marls and pure siliciclastic levels formed by deltaic progradation. The lower limit of this sequence is equivalent to the contact between the Arguis and Belsué-Atarés fms. The upper limit

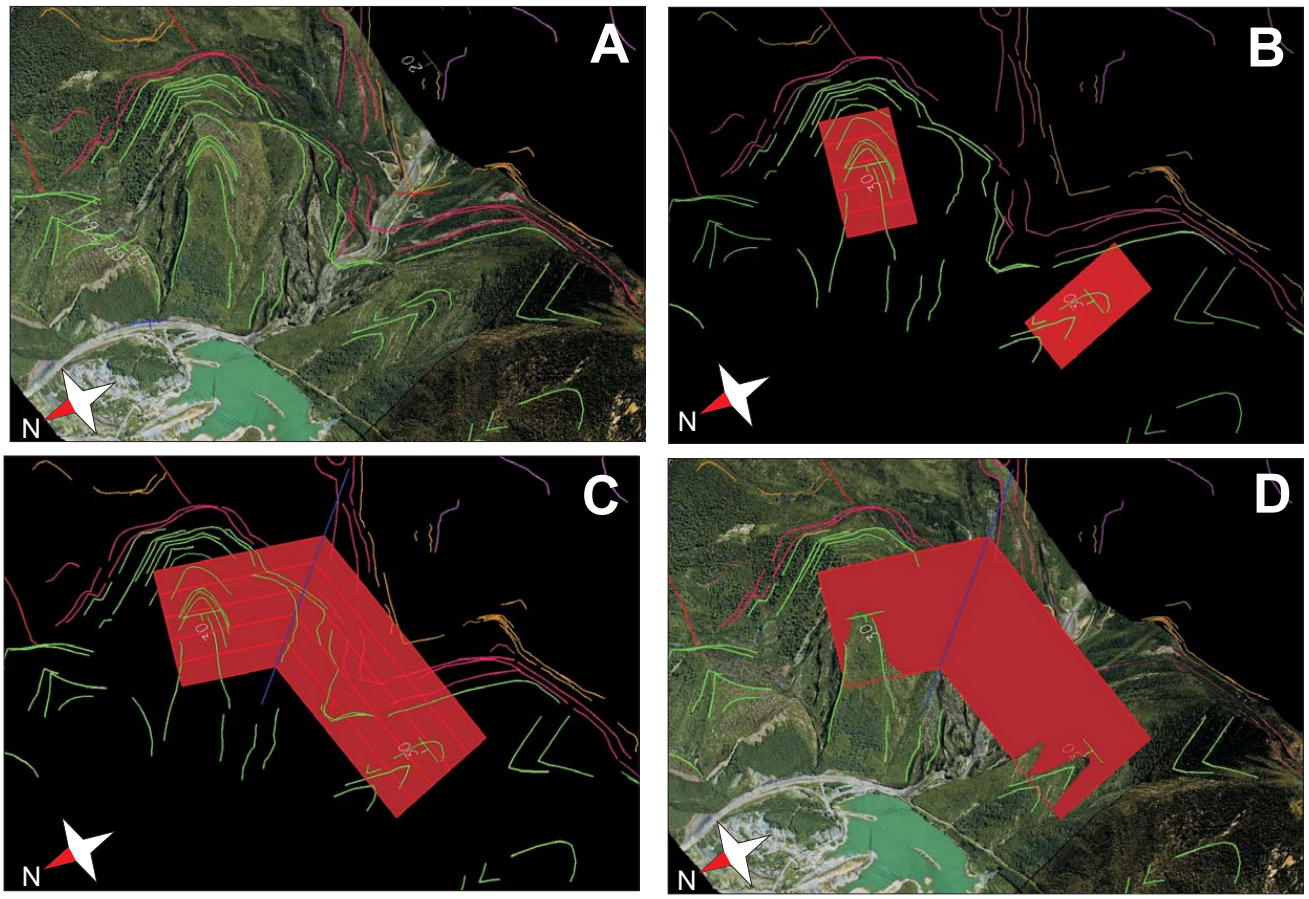

FIGURE 5 | Sketches summarizing the procedure followed in the creation of the 3D reconstruction: A) positioning of the dip data, B) creation of the dip domains, definition of the extension, C) intersection of the dip domains, and generation of the map of structural contours, and D) generation of the surface.

is a regional unconformity, recognizable all along the South-Pyrenean basin, and corresponding to the contact between the Belsué-Atarés and Campodarbe Fms. (Fig. 2). This unconformity represents a sharp transition to continental depositional environments.

3D-RECONSTRUCTION OF THE PICO DEL ÁGUILA ANTICLINE

Methodology of reconstruction

The reconstruction of the Pico del Águila anticline is based on surface and subsurface data, which have been integrated in a 3D GIS framework. The acquired data at surface comprise dip measurements, fault traces and a detailed field mapping of bedding traces within the growth strata record. These data were positioned in 3D onto a Digital Elevation Model of the area with resolution ±2.5m. The Pico del Águila anticline was reconstructed by applying the Dip Domain Method (Fernández *et al.*, 2004; Fernández, 2004), which simplifies geometries to volumes in which bedding attitude is constant (Fig. 5). To apply the dip-domain method, a comprehensive geometrical model must be established from the available data. This geometrical model must include: i) a definition of dip domains (average bedding attitude of the domain and polarity, position, and extent of boundaries); and ii) a definition of 3D stratigraphic geometries (a model of stratigraphic separations between different horizons). A totality of 91 dip domains have been defined for the top of the Guara Fm., assuming ±5º in strike direction and ±3º in dip value as a tolerance limit between domains. By intersecting the adjacent dip domains, the map of structural contours is obtained. From this, the interpolation of the structural contours was performed in the software GOCAD (Paradigm™), obtaining a smoother geometry of the reference surface that honours all the input data. The rest of the pre-folding surfaces were reconstructed using a tool in 3DMove (Midland Valley Exploration) that enables creating new folded surfaces from an existing one, for parallel and similar folds. Since the Pico del Águila is considered a kilometric-scale parallel fold (Millán, 1995), the parallel fold tool was used to reconstruct the geometry of the Triassic, Upper Cretaceous and Garumnian top

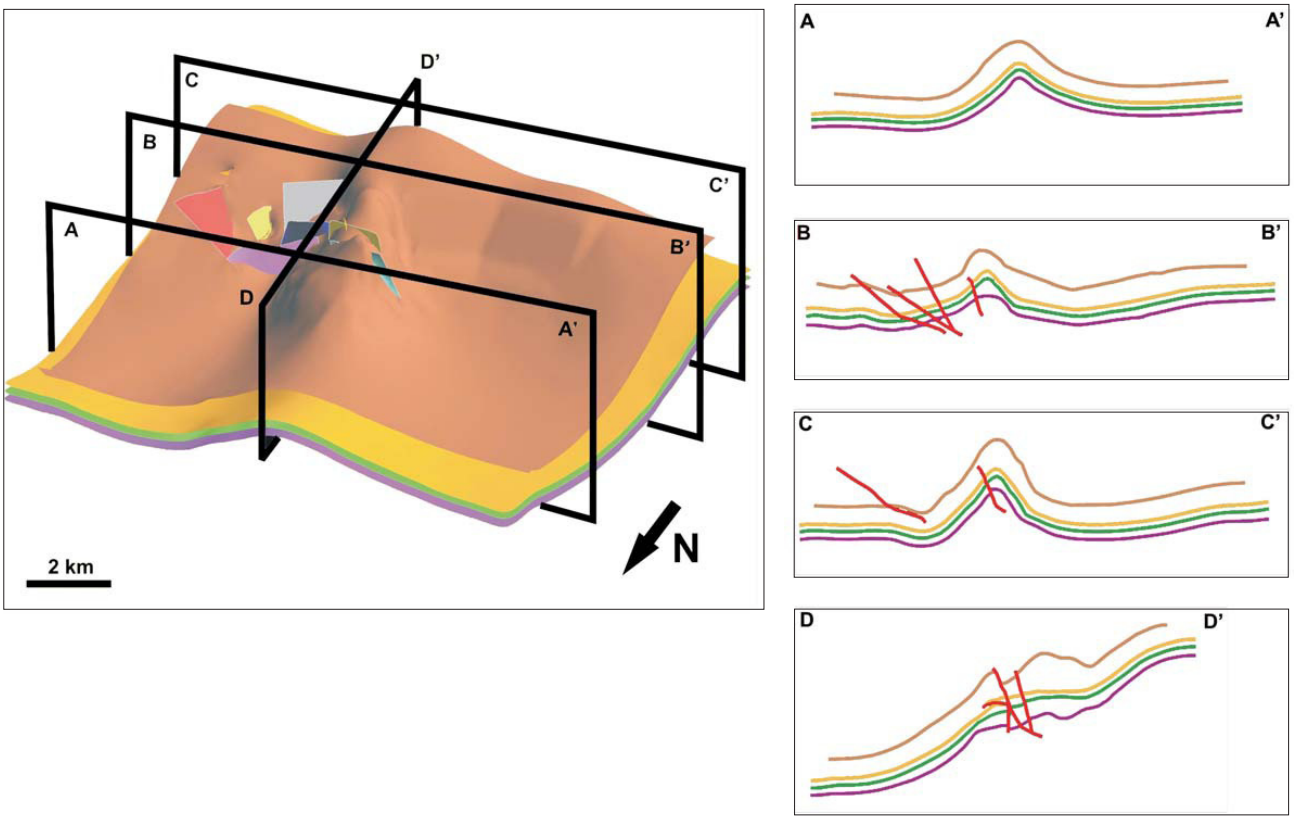

FIGURE 6 | Several cross-sections of the Pico del Águila anticline showing the structure of the pre-folding sequence . Brown: Top of Guara Fm.; Yellow: Top of Garum facies; Green: Top of Upper Cretaceous; Purple: Top of Triassic materials; Diverse colours (red in the cross sections): internal faults affecting the structure.

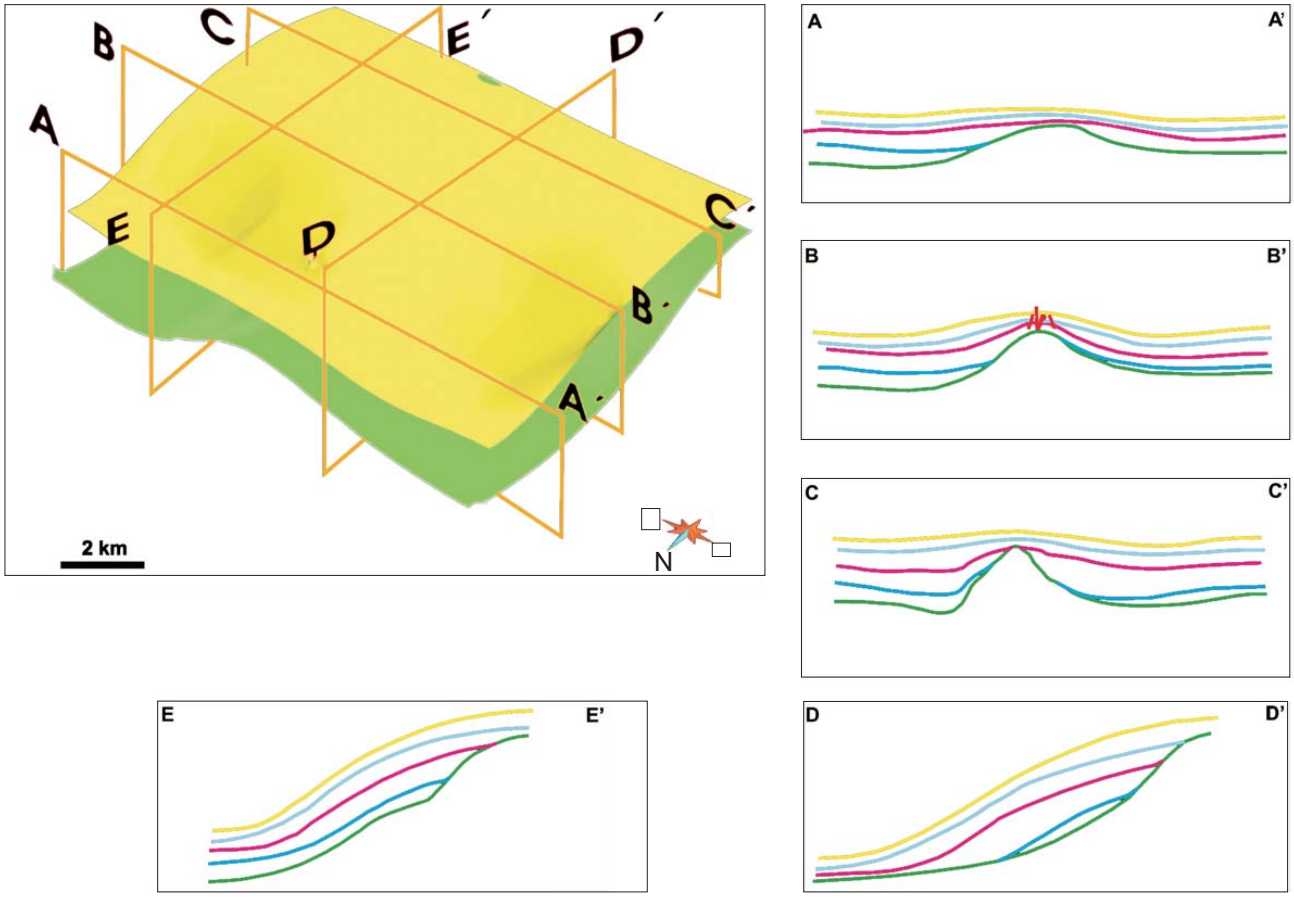

FIGURE 7 | Cross sections along and across the 3D model, showing the geometry of the reconstructed syn-folding units (top of the four major depositional sequences described in the area within the Arguis Fm.). Notice how the units thin towards the crest of the anticline and how the first depositional sequence does not reach the anticline's crest. From bottom to top units: Green: Guara Fm. (shown for reference); Blue: Growth Sequence I; Pink: Growth Sequence II; Light Blue: Growth Sequence III; Yellow: Growth Sequence IV.

surfaces. The syn-folding surfaces were constructed individually applying the Dip Domain Method. To control the variation in thickness, this study has benefited from the excellent exposure of the growth strata and the stratigraphic logs taken from Millán *et al.* (1994).

Subsurface data consist of several seismic profiles which have been interpreted to understand the structure in depth and validate the field interpretations. Due to the poor resolution of the seimic data, only the general features of the pre-folding sequence were interpreted, as well as the geometry of the South-Pyrenean frontal thrust. The seismic interpretation was then converted to depth using the interval velocity of each unit as deduced from an exploratory well outside the area and the common depth points of the seismic profiles. This information was brought to the reference 3D framework, in order to correlate the different profiles. A map of structural contours in 3D was then created for each fault/horizon. In case of the pre-folding stratigraphic horizons, the new data was attached as control points at depth to the corresponding contour map.

Results of the 3D Reconstruction

Eight stratigraphic horizons and nine faults were reconstructed. For the pre-folding sequence, four top horizons were reconstructed (Fig. 6): i) the Guara Fm. (reference surface of the fold); ii) the Garumnian facies (Cretaceous-Tertiary transition); iii) the Upper Cretaceous; and iv) the Triassic rocks. Within the syn-folding sequence, the top of the four main depositional sequences within the Arguis and Belsué-Atarés fms. were reconstructed (GS-I to IV; Figs. 7, 8). Eight fault surfaces and an internal N-S thrust as well as the geometry of the South-Pyrenean frontal thrust were reconstructed.

The geometry of the South-Pyrenean frontal thrust surface consists of a ramp that dips towards the N, ranging

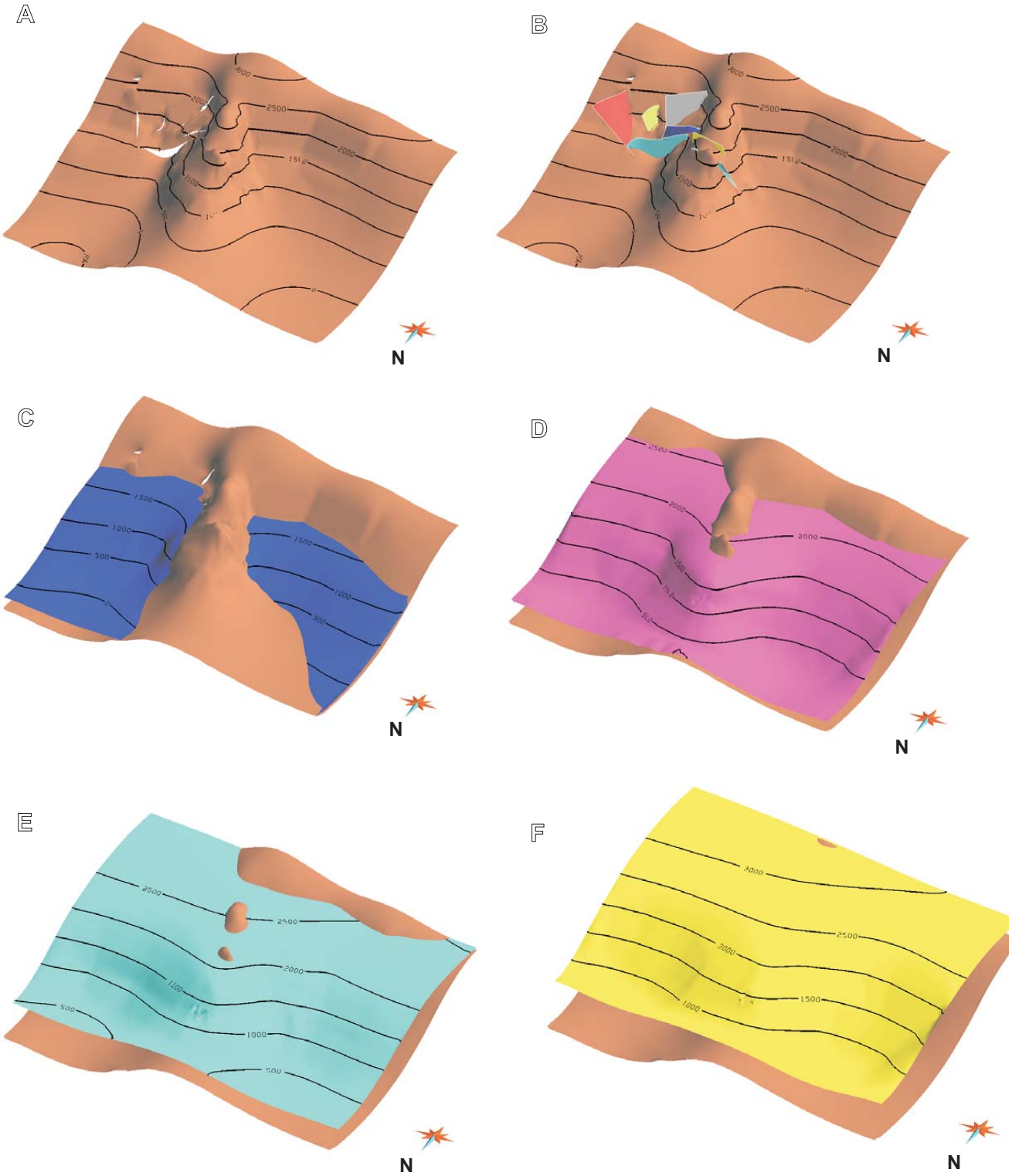

FIGURE 8 | 3D views of the reconstructed syn-folding depositional sequences. A) Top of Guara Fm. (reference surface; in brown in Fig. 6) for reference; B) Top of Guara Fm. plus the inner reconstructed faults; C) Top of Guara Fm. covered by Depositional Sequence I; D) Top of Guara Fm. covered by Depositional Sequence II; E) Top of Guara Fm. covered by Depositional Sequence III; and F) Top of Guara Fm. covered by Depositional Sequence IV.

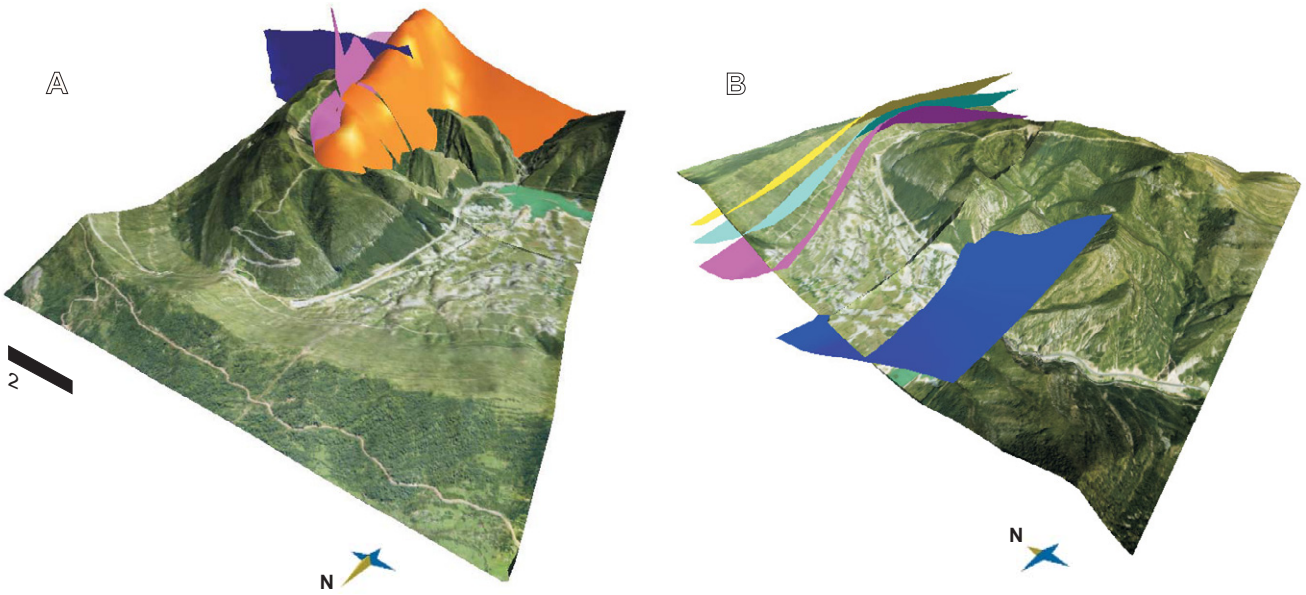

FIGURE 9 | Oblique images of the Pico del Águila anticline. A) shows the interference between the anticline (Garumnian horizon in orange), the set of NNE-SSW to E-W faults (dark blue), and the N-S internal thrust (pink); B) shows the geometry of the growth strata (sequences I to IV) intersecting the topography and thinning towards the periclinal closure defined by the Guara limestones.

from 15º in the rear part to 37º in the frontal emerging zone, and a sub-horizontal flat extending to the north, beyond the studied area (Teixell and García-Sansegundo, 1995; Oliva and Pueyo, 2007). The top of the Guara Fm. is barely affected by the set of faults and unconformably overlies the N-S thrust. The lower units, however, display a complex structural pattern due to the interference between the faults (E-W to NNE-SSW striking) and the N-S trending thrust (Fig. 6).

The syn-folding sequence displays a gentler geometry, characterized by thinning towards the crest of the anticline and upwards decrease in the intensity of deformation (Figs. 7, 8, 9B). GS-I does not reach the crest of the anticline and onlaps onto both flanks. The upper depositional sequences progressively cover the top of the Guara Fm. (Figs. 7; 8).

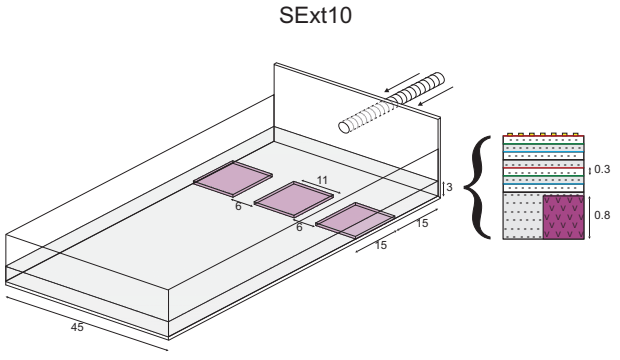

FIGURE 10 | Initial setup of the analogue model SExt10 presented in this work, showing the distribution of ductile (SGM-36; three grey squares within the modelling box) and brittle (sand) décollements and the shortening orientation. The stratigraphic sequence of each model is presented aside. All values are in cm (From Vidal-Royo *et al.,* 2009).

ANALOGUE MODELLING: GENERATION OF OROGEN-PERPENDICULAR THRUSTS

The analogue models aim to test the effect of variations in rheology of the basal décollement as a factor controlling the generation of orogen-oblique and orogen-transverse structures such as the ones observed in the central External Sierras. The experimental design is based on field observations which indicate a nearly absence of Keuper facies in the core of the transverse anticlines (*e.g.*, Pico del Águila and Gabardiella anticlines, Fig. 1), and thicker evaporite layers in between, where the orogen-parallel structures develop (*e.g.*, South-Pyrenean thrust front). The aim of this irregularly distributed detachment level was to show how lateral contrasts in friction were able to cause the generation of arcuate, oblique and even transverse structures during a single shortening event.

Initial setup, materials and modelling strategy

The model presented in this section was labelled model SExt10 (Vidal-Royo *et al.*, 2009). The initial setup is a colour inter-layered sequence of sand covering an uneven basal level made of three transparent silicone patches adjacent to pure brittle sand (Fig. 10). Dry quartz sand with a density of 1700kg/m^{-3}, cohesive strength C of ca. 140Pa

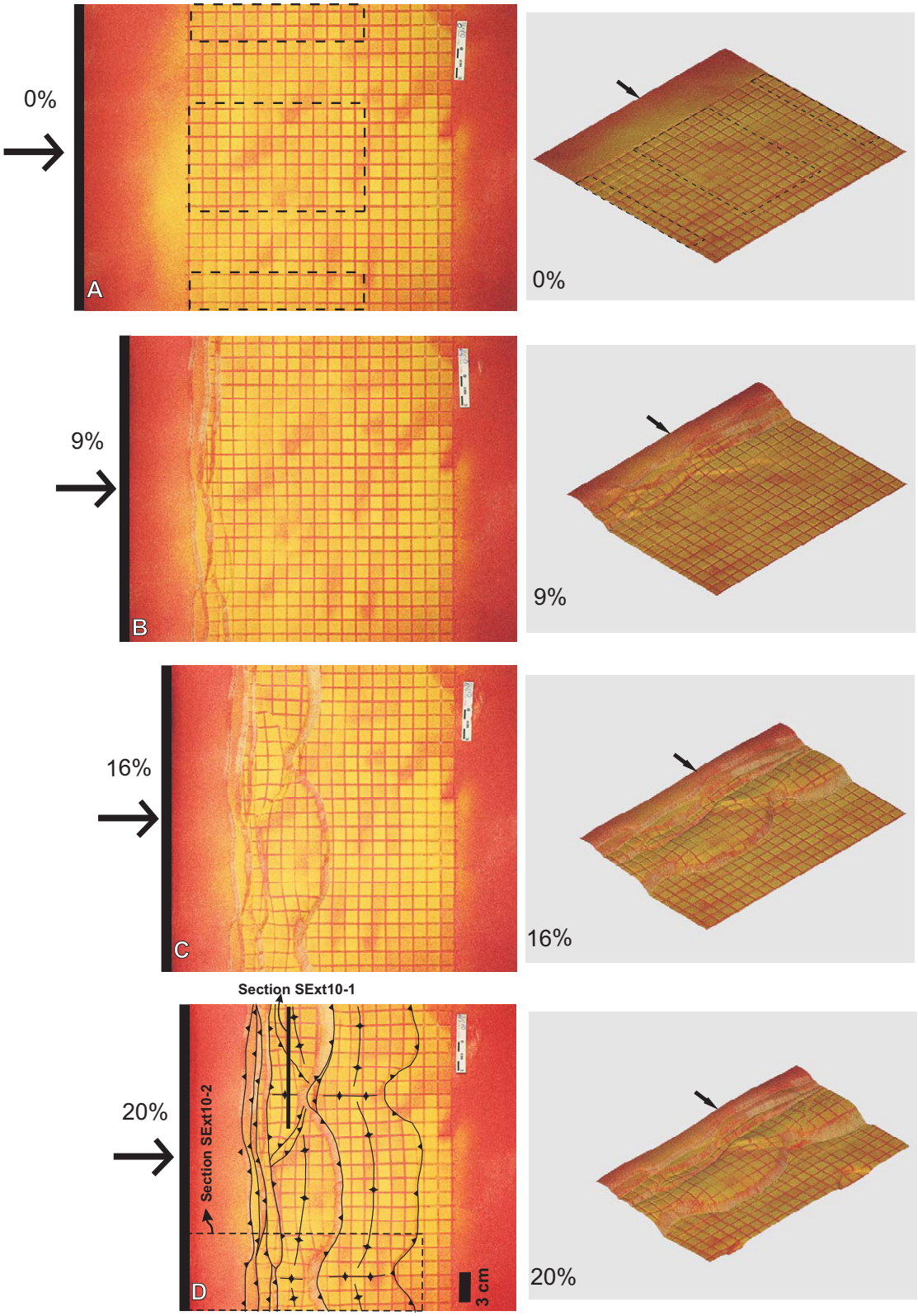

FIGURE 11 | Top and 3D views of the analogue modelling experiment at different stages: A) non-deformed stage (dashed rectangles indicate the initial position of the silicon patches); B) after 9% of shortening; C) after 16% of shortening; D) after 20% of shortening. The arrows indicate the orientation and sense of shortening. Dashed rectangles in A) indicate the initial position of the ductile layers in the basal décollement. Dashed rectangle in D) indicates the location of horizontal section SExt10-2 shown in Figure 12.

and sieved to an average grain size of 35μm was used to simulate the brittle sedimentary cover of Upper Cretaceous to Lutetian rocks. The Triassic irregular detachment level was simulated by means of the Newtonian viscous silicone putty SGM36 (density of 987kg m-3 and effective viscosity η of 5x104Pa s at room temperature, manufactured by Dow Corning Ltd.) adjacent to dry quartz sand.

The deformation rig sat upon a glued-sand aluminium plate. The model had a fixed width of 45cm an initial length of 60cm, and a constant detachment thickness of 8mm (Fig. 10). Our intention by gluing sand onto the basal plate was to force high friction behaviour in the basement in order to accentuate the contrast between the ductile décollement (silicone layers) and the frictional décollement (sand). Compression was applied at a rate of 1.85cm/h^{-1}(5.13x10-6m/s^{-1}) from one side using a motor-driven worm screw (Fig. 10). The model was shortened by up to 20% during 6h.

Results from analogue models

Shortening of the models caused deformation in both the sand and the silicone layers. The deformation pattern was different between areas detached on the frictional décollement (sand detachment; HF-High Friction areas) and areas detached on the ductile décollement (silicone detachment; LF-Low Friction areas). Deformation starts developing three frontward thrusts, since the deformation front has not yet reached the silicon patches. After 9% of shortening (Fig. 11B), deformation reaches the silicon patches, creating a clear differential advance between areas detaching on silicon and areas detaching on sand. The HF areas show additional uplift with respect to LF areas, occasionally expressed via some local oblique thrusts that merge with the main straight frontal thrusts in the rear part of the model. After 16% of shortening (Fig. 11C), structures are not able to accommodate more deformation and the front migrates frontwards. Consequently, a second generation of parallel-to-shortening structures is formed (shown on Fig. 11C). The location of the thrust front in the LF areas coincides with the frontal tip line of the silicon patches. After 20% of shortening (Fig. 11D), the HF areas do not advance as far as the LF areas do, creating a structural pattern constituted by wavy thrusts that transport the areas detached on silicone further than the areas detached on sand.

The deformation of the more plastic silicone putty layers by flow, ductile thickening and folding is laterally transferred to HF areas, where lateral thrust ramps climb up-section from the ductile layers at their lateral pinch-outs. These lateral ramps merge in the core of the HF areas, uplifting and gently deforming the units above, and highly faulting the units below (Fig. 12A, B). This results in a lateral migration of ductile layers towards HF areas and the thickening along the HF/LF boundary where the lateral

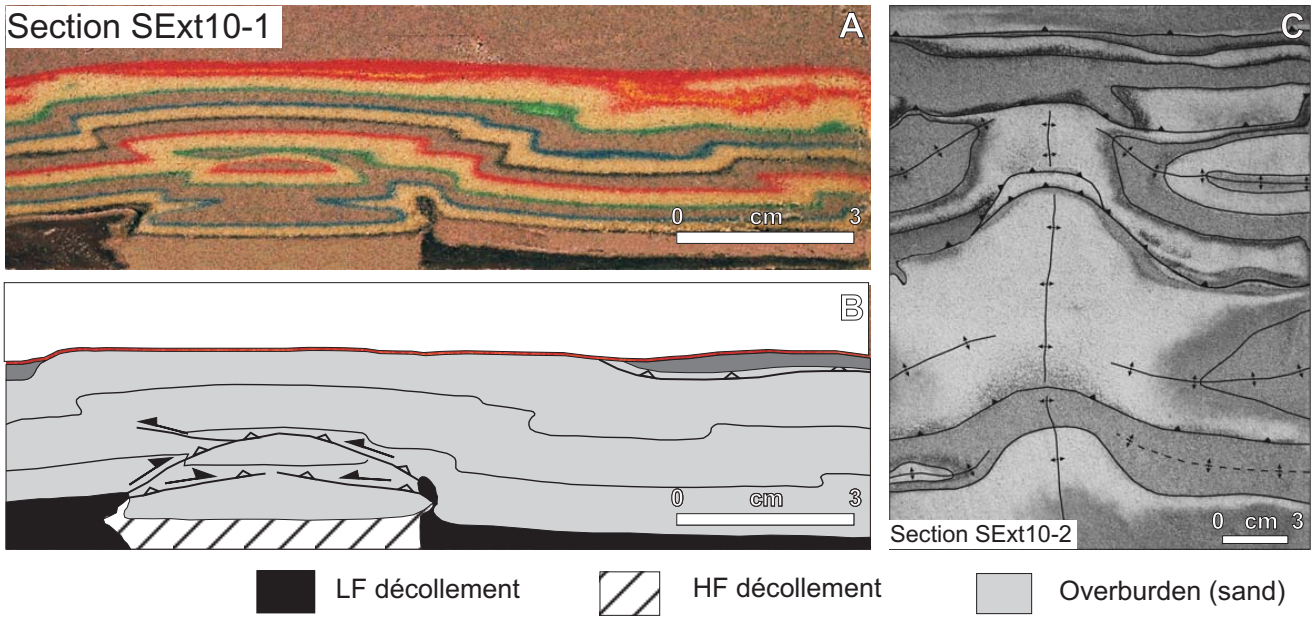

FIGURE 12 | Pictures and line-drawings of a perpendicular-to-shortening and a horizontal sections of model SExt10 (see Fig. 11D for their location). Section SExt10-1 shows the additional uplift of HF areas with regard to LF areas. Deformation is accommodated by high faulting in the lower units and by gentle folding and small oblique reverse faults in the upper units (the small faults caused for the pure brittle behaviour of loose dry sand). Notice the thickening of ductile layers towards HF areas, and how lateral ramps detach on LF/HF limits and merge in the core of the structure, uplifting the upper units. Section SExt10-2 shows the interference structural pattern between orogen-parallel and transverse structures. This section provides valuable information, allowing to observe how units modify their geometry when the behaviour of the basal décollement changes.

ramps detach (Fig. 12A, B). In horizontal sections, where the internal geometry of the layers is shown at depth, the layers show general foreland-directed thrusts in which lower units are thrusted and upper units are gently folded. Only a periclinal closure is observed on the orogen-side of the transverse structures (Fig. 12C). This indicates that these structures slightly plunge towards the hinterland owing to the tilting created by the emplacement of the frontal foreland-directed thrust.

Therefore, areas detaching on sand partially accommodate the deformation by an additional uplift with regard to areas detaching on silicon, developing gentle transverse anticlines in the hangingwall of the thrusts. The location of their crest fits almost exactly with the centre of the HF areas. This indicates that the contrast in friction between silicon and sand along the shortening direction has acted as a buttress, nucleating the thrust generation in the tip line of the silicon patches.

NUMERICAL MODELLING: ROLE OF MECHANICAL STRATIGRAPHY AND SYN-KINEMATIC SEDIMENTATION

This section presents results from a numerical model that has been used to understand the contribution of a complex mechanical stratigraphy and syn-kinematic sedimentation in the growth of the Pico del Águila detachment anticline. A two-dimensional Discrete Element Modelling technique has been used.

This method treats a rock mass as an assemblage of circular elements connected in pairs by breakable springs or bonds (Hardy and Finch, 2005, 2007). Thus, it is possible to model different mechanical properties (*e.g.*, a stratigraphic sequence) by assigning different values of breaking threshold to each pair of elements (cf. Hardy and Finch, 2005). This allows us to test the effect of a given mechanical stratigraphy on geometry, fold kinematics and folding mechanisms. As such, the method provides more information than previous kinematic modelling approaches. Furthermore, it allows for easy monitoring of displacement/location of the elements through time. In this way, the displacement path, the kinematic evolution and the strain distribution within the body can be easily tracked at any stage of the modelling. Given the competent/incompetent interlayering that characterizes the stratigraphic record (Fig. 2), we believe it is an ideal method with which to model the Pico del Águila anticline.

As explained previously, the Pico del Águila provides a well-exposed down-plunge view of a fold down to the Triassic core, along with a well described mechanical stratigraphy and spectacular growth strata that record the fold development. This provides an excellent basis to compare how the mechanical stratigraphy behaved in the natural fold vs. the model, and how the syn-kinematic sedimentation influenced the fold's evolution.

Initial setup and experimental parameters

The behaviour of the simulated rock mass is broadly elasto-plastic and frictionless between the circular elements (Place and Mora, 2001; Finch *et al.*, 2003, 2004; Hardy and Finch, 2005, 2007), an approach used in previous studies to model the brittle deformation in sedimentary rocks in the upper crust. Deformation of the modelled sedimentary

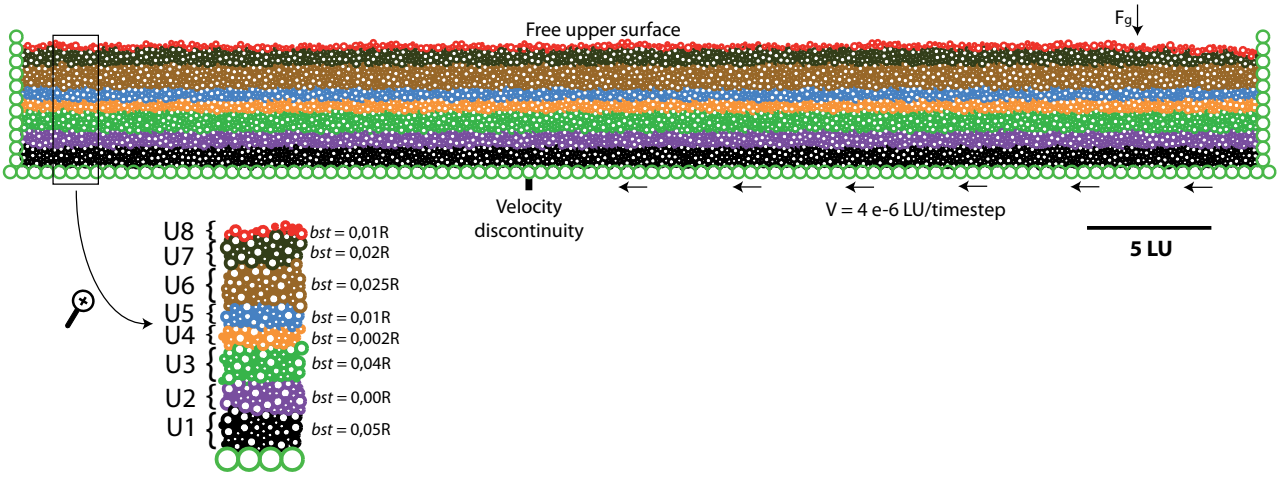

FIGURE 13 | Initial setup and boundary conditions applied in the DEM experiment. The initial assembly contains 10245 elements with radii of 31.25, 25, 18.75, and 12.5m, positioned at random in a box that measures 12.5x1.25km. The assemblage is composed of 32 flat-lying layers that are later grouped in eight units with different mechanical properties (bst: Breaking strength between pairs of particles). Displacement is increased at 0.001m/time-step. Fg corresponds to the force of gravity.

sequence occurs in response to shortening at a subduction slot at the base of the model (a common configuration in sandbox experiments). A velocity discontinuity is created at the subduction slot in the central basal part of the box, in which the right half of the model moves leftwards at a continuous rate of 0.001m per time step (Fig. 13). A homogeneous rock density of 2500kg m^{-3} has been used, a typical value of upper-crustal sedimentary rocks (Hardy and Finch, 2005). A value of 5.5x109N m^{-2} is used for the elastic constant (K) in the experiments. The experiment was run for 2,000,000 time steps with output of the assembly every 100,000 steps (*i.e.*, every 100m shortening). This provided a precise control on the structural evolution and variation of the strain distribution and a well constrained geometry of the syn-kinematic sedimentation. The total model displacement was 2km.

Within the modelling framework, one lattice unit corresponds to 250 metres. The initial particle assembly contains 10,245 elements with four different radii of 0.125, 0.1, 0.075 and 0.05 lattice unit (*i.e.*, 31.25, 25, 18.75 and 12.5m, respectively) distributed at random in an enclosed rectangular box. These dimensions are considered suitable, since they provide enough resolution to model a kilometric-scale structure like the Pico del Águila anticline, avoiding the generation of preferred planes of weakness and allowing a non-predefined localisation of deformation that a homogeneous isotropic particle size would imply. After initial generation, the elements are allowed to relax to a stable equilibrium and are left to settle under gravity for ~2,000,000 time steps to obtain a stable, well-packed initial assemblage and to further minimise void space. The resulting initial assembly is 12.5km long and ca. 1.25km thick, simulating a continuous rock mass that can deform by progressive bond breakage (fracturing/faulting) and bulk motion of unbroken pairs of elements (folding). The syn-kinematic sedimentary sequence was modelled by adding incrementally a total of 11,708 elements. The initial particle assembly was composed of 32 flat layers grouped into eight units (U1 to U8) with different mechanical

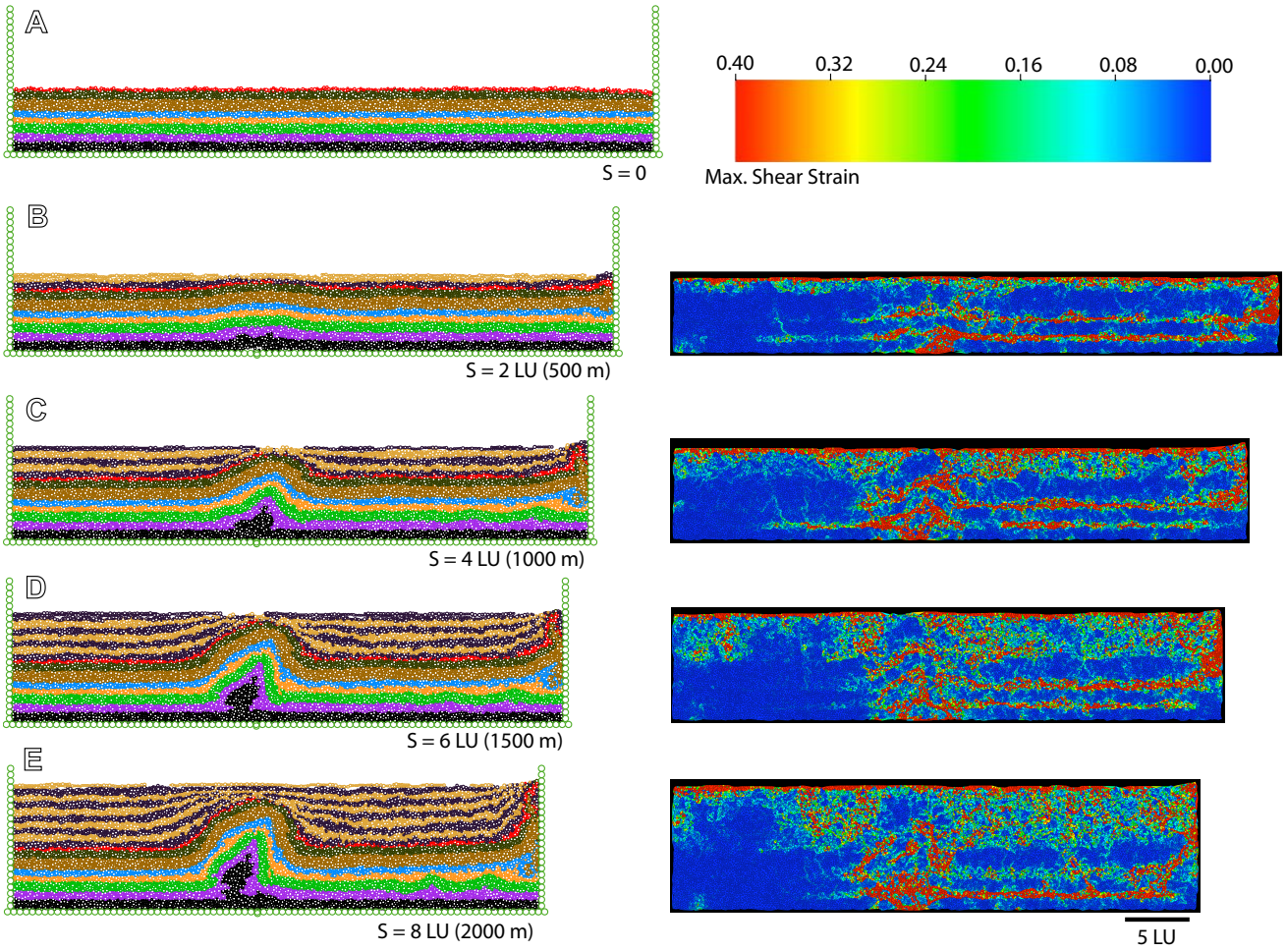

FIGURE 14 | Evolution of the DEM model shown at: A) 0m; B) 500m; C) 1000m; D) 1500m; and E) 2000m. The left column illustrates the geometrical evolution of the model as shortening progresses. The right column shows the distribution of the shear strain at the reported stages. Scale at the top-right of the figure illustrates the range of average shear strain considered.

properties to create a complex mechanical stratigraphy (Fig. 13) that modelled the stratigraphic column described in the field. The selected values (Fig. 13) have been chosen based on the uniaxial compression tests carried out in Hardy and Finch (2007).

Results from numerical models

The geometrical and shear strain evolution of this model are shown in Figure 14.

After 4% bulk shortening (500m; Fig. 14B) a small, low amplitude antiform has started to grow above the velocity discontinuity as a perturbation with layer-parallel geometry. The incompetent units U2 and U4 exhibit high shear strain in both the structure itself and some distance across the model. Competent unit U1 shows high shear strain and is complexly deformed in the core of the anticline. The other pre-kinematic units only exhibit low shear strain, which is slightly accentuated in the fold (Fig. 14B). The growth strata show high but variable amounts of shear strain. However, two types of strain within the growth strata package must be distinguished. Firstly, the shear strain due to the recent deposition and ongoing compaction of the recently deposited units (essentially restricted to the uppermost two layers of the assembly; *i.e.*, the thin horizontal red area at the top of the strain distribution maps; Fig. 14). Secondly, the shear strain exhibited by the growth pile due to shortening and consequent fold development. A border-effect is generated at the right-hand edge of the model due to the displacement of this wall towards the left. After 8% bulk shortening (1000m; Fig. 14C), the central structure has grown significantly, its limbs have steepened and now it verges slightly towards the right. Disharmonic folding is observed. Below U4 minor folds have developed, particularly in U2-U4 towards the right-hand edge of the model, and the core of the structure is now becoming complexly deformed in U1. Above U4, the pre-kinematic units define a gentler fold geometry. The syn-kinematic sequence shows marked thickness variations producing flanking sedimentary wedges which thin towards the crest of the anticline. Within the growth strata package, moderate to high shear strain is observed and a distinct contrast in shear strain is observed at the base of the growth strata package. After 12% bulk shortening (1500m; Fig. 14D), thickening of the incompetent units is seen in the hinge of both flanking synclines and the core of the fold becomes highly deformed. In particular, U1 starts to become dramatically deformed, displaying bottle-neck geometry. Small folds continue to grow in U2 between the anticline and the right-hand model border. Disharmonic folding is observed in the hinge of the anticline, with large differences in folding style above and below U4. Shear strain continues to be concentrated within the incompetent units. Growth strata rotate and thin against the growing structure displaying much internal shear strain. At 16% bulk shortening (2000m; Fig. 14E) the upwards growth of the anticline appears to cease (growth strata overlap the structure) with the fold tightening by limb rotation. However, the model shows a shift in the distribution of shortening from the central fold to the right edge, manifested by propagation of folding from the right edge, and giving rise to small décollement folds detached on U2. In the main fold, shear strain is still concentrated in the core, as well as in the limbs particularly in U4 and U5. In the core, U1 is further "pinched" into a bottle-neck structure. At this stage, the growth strata package is about 1.2km thick, similar to the one observed in nature at the Pico del Águila.

3D GEOMECHANICAL RESTORATION OF THE PICO DEL ÁGUILA ANTICLINE

The restoration of the 3D reconstruction showed previously allows to better understand how a complex structure in 3D such as the Pico del Águila anticline evolved through time, as well as to extrapolate the complexity of the folding mechanisms found by the Discrete Element Modelling (DEM) model to the third dimension. The restoration has been done using a Finite Element Modelling (FEM) algorithm which considers measurable mechanical properties of the rocks (what has been called geomechanical restoration) rather than any imposed kinematical criteria. In most cases the kinematics of a structure are unknown or not precisely quantified, and the geomechanical restoration delivers a mechanically stable result based on the geometry of the deformed stage and the mechanical properties of the rocks (such as density, Young modulus, Poisson's ratio or porosity, among others; Maerten and Maerten, 2006; Guzofski *et al.*, 2009).

Methodology and initial setup

The sequential restoration of The Pico del Águila anticline was done using Dynel3D (provided by Igeoss). Maerten and Maerten, 2006). The code implemented in Dynel3D is based on the finite element method, a continuum technique that allows the study of natural deformation based on the mechanical properties of rocks. Although strictly elastic, the program is suitable to model the development and behaviour of complex geological structures such as folds and faults (Maerten and Maerten, 2006). The stratigraphic units are discretized with tetrahedral elements that are assigned elastic properties. Faults are represented by contact surfaces. The tetrahedral elements deform elastically in response to constraints such as applied and/or internal forces, displacements, and interface contact regions (faults). Dynel3D uses

TABLE 1 | Mechanical properties used to restore the Pico del Águila anticline

Unit	Predominant Lithology	Young's Modulus (Pa)	Poisson's ratio	Density (Kg/m^3)
GS-IV*	Sandstone	2.2 e+10	0.24	2480
GS-III*	Marlish Sandstones	2.2 e+10	0.24	2480
GS-II*	Marls	2.8 e+10	0.14	2530
GS-I*	Marls	2.8 e+10	0.14	2530
Guara	Limestones	4.8 e+10	0.25	2500
Garumnian-Cretaceous	Mudstones-Limestones	2.8 e+10	0.14	2530
Triassic	Dolomitic Limestones	4.8 e+10	0.25	2500

These are average values for each rock type, and partially based on field indications

* GS: Growth strata; Arguis and Belsué-Atarés fms.

an iterative, explicit solver that allows forces to be transmitted from node to node through the entire system until equilibrium is reached. This formulation is well suited to model complex geological scenarios that comprise several stages, such as structural restoration (Maerten and Maerten, 2006).

The 3D reconstruction of the Pico del Águila anticline was taken as the deformed stage to restore. The reconstructed growth strata were key to constrain the timing of the restoration. The average side length of the tetrahedra was 310m, a reasonable balance to represent a kilometre-scale structure without exceeding the memory allocation threshold allowed by a regular desktop computer. This average side length implies that bodies with dimensions below the threshold are not represented, being simplified in bodies of larger dimensions. That is the case of the Garumnian and the Upper Cretaceous (thickness below the average side length), which were merged into a unique mechanical unit named Garumnian-Cretaceous, with averaged mechanical properties (continuum transition from limestones to continental mudstones). Similarly, the eight internal faults exhibit a heave that barely exceeds several tens of meters. Thus, they were not included in the restoration. As said, the algorithm run in Dynel3D needs several rock mechanical properties to be set up (Young's modulus, Poisson's ratio and density). As these properties vary with lithology along the stratigraphic sequence, different values were established with regard to the predominant lithology of each unit. These values are listed in Table 1.

Results from the 3D Geomechanical Restoration

Five restoration stages were considered, following the reconstruction of the four top bounding surfaces of the growth depositional sequences (GS-I to IV) and the top of the Guara Fm. (Fig. 15). The distribution of average shear strain (abbreviated as strain from now on) for each restoration step was also plotted to track the evolution of the deformation (Fig. 16). Restoration of the top of the GS-IV (36.6Myr) removes most of the tilting associated to the emplacement of the South-Pyrenean frontal thrust (Fig. 15A, B). A ca. 15º vertical axis clockwise rotation is observed. Strain is distributed heterogeneously throughout the model (Fig. 16B). GS-IV displays moderate to high strain distributed around the associated synclines, increasing progressively towards the anticline (higher strain values coinciding with areas in which GS-IV is thinner; Fig. 16B). The rest of the growth sequences display high strain in the hinge area of the synclines. Within the pre-folding sequence, the Garumnian-Cretaceous and Triassic exhibit high strain in the hinge areas of the anticline and the synclines. The Guara Fm. displays low to moderate strain along both fold flanks, and high strain in the hinge of the synclines (Fig. 16B).

The GS-III (37.17Myr) is the first restored growth unit that does not cover all the anticline. Restoration of this sequence results in a plunge decrease of 4º (Fig. 15C) and a clockwise rotation of 2º. Low to moderate strain in the hinge of the anticline at GS-III and low strain in the rest of the growth sequences is observed. The highest strain is accommodated by the Guara Fm. in the eastern syncline and along the western limb (Fig. 16C). The Garum-Cretaceous displays moderate to high strain and pronounced layer-parallel slip with respect to the units above and below. The Triassic exhibits moderate to high strain, more concentrated in the middle sequence of the synclines and anticline hinges.

After restoring GS-II (37.74Myr), the plunge almost disappeared (Fig. 15D) and the structure rotated ca. 10º additional degrees. The strain (Fig. 16D) is higher than

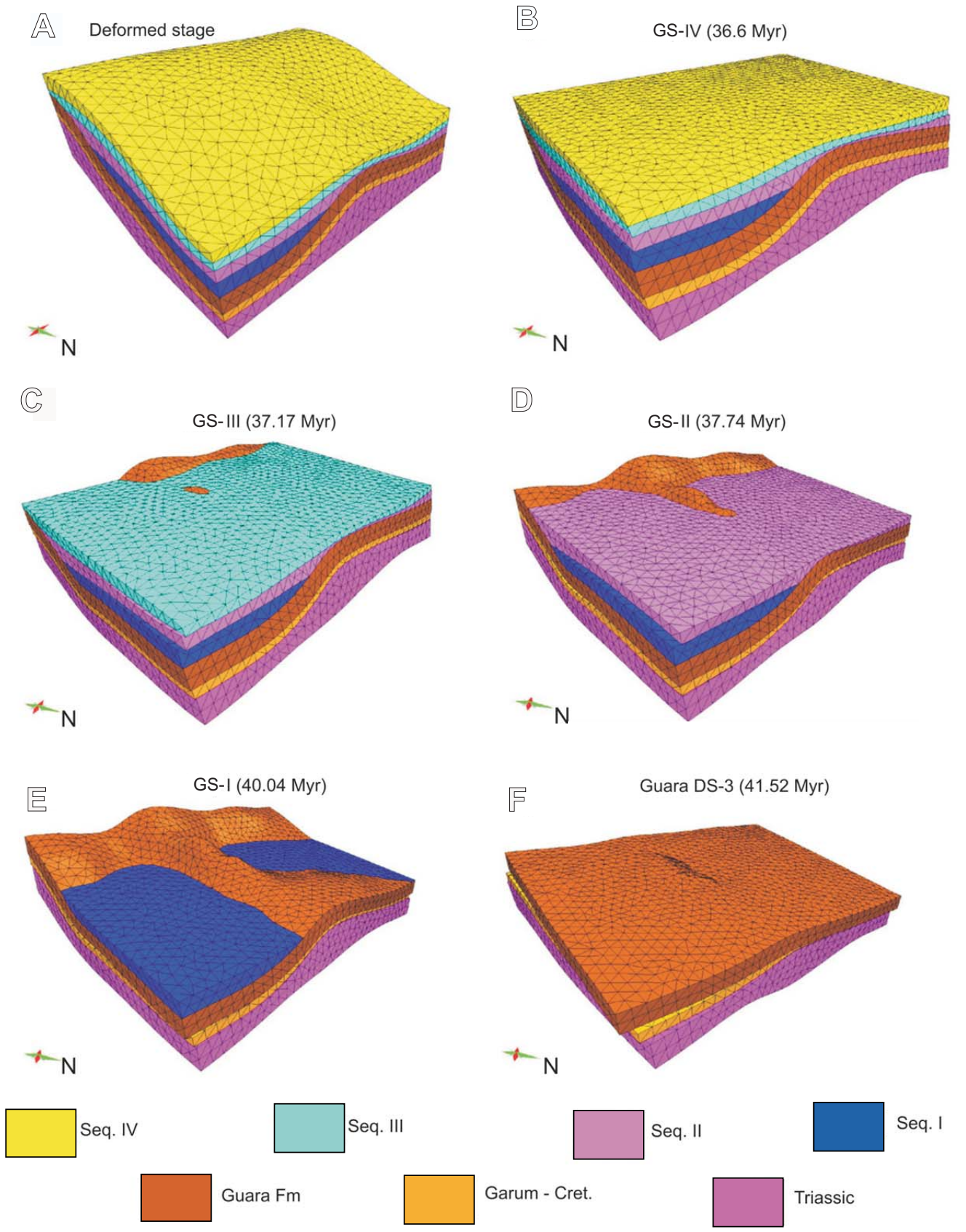

FIGURE 15 | Sequential, geomechanical restoration of The Pico del Águila anticline. A) Deformed stage; B) Restoration of GS-IV (36.6Myr); C) Restoration of GS-III (37.17Myr); D) Restoration of GS-II (37.74Myr); E) Restoration of GS-I (40.04Myr); and F) Restoration of Guara Fm. (41.52Myr).

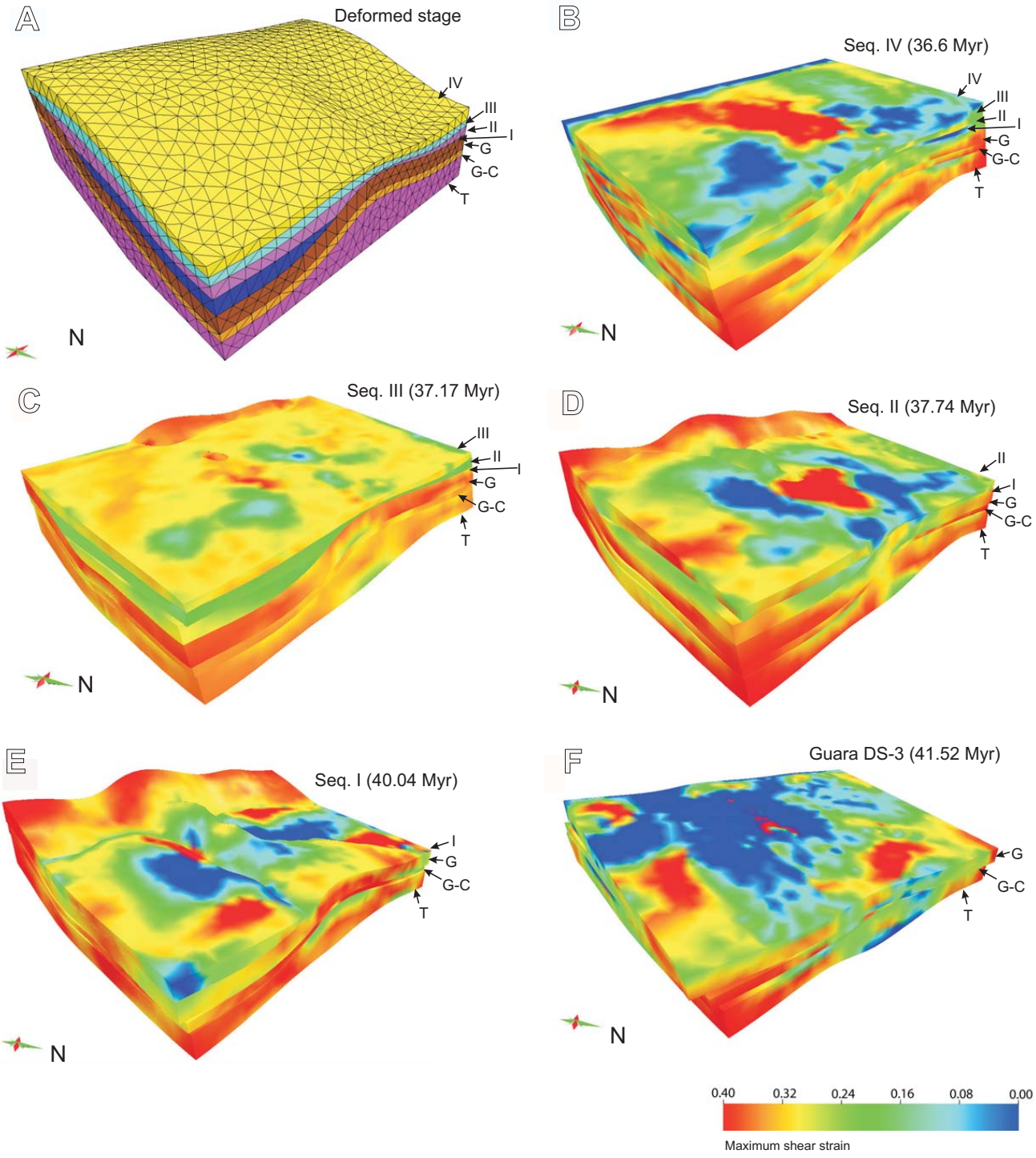

FIGURE 16 | Average shear strain between the restoration steps shown in Figure 15: A) Deformed stage geometry for reference; B) Restoration of GS-IV (36.6Myr); C) Restoration of GS-III (37.17Myr); D) Restoration of GS-II (37.74Myr); E) Restoration of GS-I (40.04Myr); and F) Restoration of Guara Fm. (41.52Myr). T: Triassic; G-C: Garumnian Cretaceous; G: Guara; I: GS-I; II: GS-II; III: GS-III; IV: GS-IV.

in the previous stage, particularly at the periclinal closure of the anticline. The Guara Fm. accommodated moderate strain in the western limb and the crest of the anticline, and high strain in the hinge of the eastern syncline (Fig. 16D). The Garum-Cretaceous displays high strain, except in the anticline crest. The Triassic displays moderate to high strain.

The restoration of GS-I (40.04Myr) unveils the Guara Fm. at the crest of the structure (Fig. 15E). Intense deformation is observed in the pre-folding units, displaying a well-developed anticline (Fig. 15E). No significant vertical axis rotation is observed. Strain in GS-I is heterogeneously distributed, displaying low to moderate high strain around the hinge of the synclines and along the flanks onlapping the Guara Fm. (Fig. 16E). The Guara Fm. exhibits low strain in the anticline crest and moderate strain in the periclinal closure and along the flanks. The Garumnian-Cretaceous shows particularly high in the hinge of the anticline and along the flanks. The Triassic displays moderate to high strain in the synclines and along the décollement, and low strain in the crest of the anticline (Fig. 16E).

Finally, the restoration of the Guara Fm. (41.52Myr) causes unfolding of the pre-folding sequence and additional rotation of ca. 6º (Fig. 15F). The vertical axis rotation varies through the pre-folding units, displaying a slight larger rotation of each unit with respect to the unit immediately below (Fig. 15F). The strain ranges from very low to very high, with low to moderate values throughout the model, and maximum values in the hinge of the synclines and locally in the crest of the anticline (Fig. 16F). The Garumnian-Cretaceous and Triassic display larger strain values in the hinge of the synclines (Fig. 16F). The top and bottom of the units display slightly lower strain values along their contacts, with significant layer-parallel slip between them.

DISCUSSION

On the benefits and drawbacks of each technique

Each of the presented models delivers new insights on the structural evolution of the Pico del Águila anticline, thus improving the geological knowledge of the External Sierras. Each of them was specifically designed to test certain parameters observed in the field, incorporating the contributions to the model of structural evolution. However, recognizing the limitations of each technique is essential to choose the most appropriate method for a given purpose. In such a way, one can evaluate the outcome of the model and extract the net contribution of the whole results.

Sandbox modelling was a good technique to model the heterogeneities of the basal décollement at a regional scale: it allowed an easy visualization in 3D of the model response to deformation in terms of differential advance/uplift of the overburden, structural style and relief across the different domains. Given the important changes of structural style in 3D, the analogue models represent the structural features at a regional scale. The mechanical contrast between loose sand and silicon putty was suitable to model the effect of lateral changes between Keuper and Muschelkalk facies in the Triassic décollement. The contrast effectively reproduced a larger N-S uplift (*i.e.*, parallel to shortening direction) in the areas detached on high friction décollement (HF areas) and a larger advance of the deformation front in areas detached on ductile décollement (LF areas). On the contrary, working with loose sand and silicon do not provide enough accuracy to model the internal complexity of the overburden: high contrasts in mechanical behaviour are described in the field along the stratigraphic sequence, in which inner ductile units are present and have great influence in the growth of the structure (Figs. 2; 14). To model this, a wide diversity of analogue materials would be needed, and even then, the available mechanical properties would be limited to the number of different materials used in the modelling. For this reason, it has been found more suitable to assess the role of the mechanical stratigraphy in the fold growth by means of numerical modelling.

The scaling of parameters has always been a key issue in sandbox modelling: the dimensions of the field structure, the stratigraphic thickness of units and the mechanical properties of the materials must be rescaled to accomplish similar processes at a much smaller timescale. Although not discussed herein, the suitability of the analogue materials, the rescaling factor of their physical properties and the dimensions of the experimental apparatus versus the thickness of the model units are factors that must be considered accurately when designing the initial setup of the model. For the models presented in this work, these aspects were discussed in more detail in Vidal-Royo *et al.* (2009), based on many other works such as Weijemars, 1986; Bonini, 2003; Cagnard *et al.*, 2006; Amilibia *et al.*, 2005; among others.

The morphological and structural changes of the model can be captured in real time and observed physically (Fig. 11), the advance/uplift contrasts can be easily illustrated with a simple photo camera, and a qualitative distribution of strain across the different structural domains can be derived by comparing a series of top views. However, in analogue modelling all the data must be extracted and well documented during the model run and sectioning, and the repeatability is usually much more time-consuming and less accurate than in numerical models.

The mechanical properties of the overburden, as well as the effect of the growth strata in the distribution of the strain during the fold growth can be better controlled if modelled numerically. The DEM permits a precise control of the mechanical response of each modelled unit, hence, to set up a highly complex mechanical stratigraphy with which to model a plethora of geological scenarios. This makes the DEM an ideal method to explore in detail the evolution of the N-S detachment anticlines of the central External Sierras. The method allows us to track every single particle of the model and its associated physical information (displacement, velocity and acceleration vectors, instant position, etc.) from which the distribution of strain through time is easily derived. The DEM models presented in this work have contributed with new insights on how the deformation is differentially accommodated depending on the mechanical behaviour of each unit, leading to large contrasts in structural style between adjacent units within the sedimentary cover of the Pico del Águila anticline. The numerical models allow a precise control of the parameters introduced in the model. It is important to have control of the thickness of the pre-folding units (constant thickness, set up before running the model), and even more in the case of the growth strata, to model a geological setting as described in the field. However, there are no kinematics superimposed on the model. The DEM is a forward modelling technique in which the physical properties of the particles, the initial dimensions of the bounding box and the stratigraphic thicknesses are the only introduced parameters. In this sense the DEM shares similarities with the classical sandbox models, but allows a major control of the mechanical properties and instantaneous monitoring of the kinematic parameters and strain distribution of any/all particle(s) of the assembly. On the other hand, the presented DEM models are strictly 2D, providing a partial representation of the modelled structure (comparable to an E-W cross section of the anticline). Although 3D DEM experiments are already being developed (Carmona *et al.*, 2008), they are still very expensive in terms of time consumption, especially when modelling complex geological settings such as the N-S anticlines of the central External Sierras. For this reason, a 2D DEM approach has been suitable to understand the role of the mechanical stratigraphy plus growth strata in a single structure, since the sandbox experiments had already shed light on the generation of the N-S structures in 3D at a regional scale. Technically, the DEM experiments represent one step further in modelling applied to structural geology. By means of calculations based on field observations of the mechanical response of rocks in nature, a complex mechanical interlayering can be modelled, improving the validation between model and nature with regard to more simplistic approaches such as analogue models or kinematic models that need superimposed constraints to be run. In addition, the method outputs as many intermediate steps as the modeller decides. The outcome files are stored and can be accessed later in the future for further analysis or comparisons. The repeatability of the experiments is better than in sandbox modelling.

The Pico del Águila anticline is a 3D structure with an excellent preservation of the growth strata record. The interference pattern between the N-S anticline and the E-W South Pyrenean thrust creates a structure with a complex kinematic evolution that is difficult to represent properly by means of 2D approaches. All these factors enabled the three-dimensional reconstruction of the structure plus growth strata with which to assess a time-constrained model of evolution. The good degree of exposure, outcropping conditions and the easy accessibility made it an ideal case to carry out field data acquisition and detailed mapping of geological traces. This led to a reconstruction of the pre-folding units and growth strata in 3D, which allowed the understanding of the geometry and served as a basis to carry out the restoration. Based on the mechanical response of rocks to deformation, the geomechanical-based algorithm of Dynel3D presented an alternative to perform a sequential time-constrained restoration in 3D without invoking complex and not precisely quantified (even unknown in many cases) kinematics of the structure such as shortening rate, displacement vectors and folding mechanisms. Thus, the major benefit of a geomechanical restoration is that it allows us to restore a structure by introducing real, measurable properties of the rocks without imposing any kinematic criteria. Density, Young Modulus, Poison's ratio or porosity can be measured in strength tests in the laboratory, or alternatively, general values can be found in published charts of mechanical properties for different materials. In any case, measurable or easily accessible values are used to perform a restoration that returns a physically-based result in accordance with the kinematics derived from a diversity of disciplines. The algorithm solves the system and delivers the mechanically most stable solution, letting the model move freely and unconstrained in the XYZ directions. The main drawbacks of this method, so far, link directly with the technical limitations of computer calculations. The algorithm implemented in Dynel3D may need to allocate a large amount of the computer's memory, depending on the desired resolution of the model (*i.e.*, the size of the tetrahedra). This means that for a structure of a scale of a few kilometres such as the Pico del Águila, a regular Desktop computer can stand up to a resolution of some hundreds of meters. This limitation makes the method unsuitable for detailed studies and geological features of this scale which are below the resolution threshold. The algorithm is based on the use of elasticity laws to restore large, non-recoverable (inelastic) deformation. This implies certain limitations. Particularly on the magnitude of strain, the use of elasticity laws return strain values which are notably lower than those predicted by other modelling techniques (*e.g.*, DEM) and the values obtained in field/laboratory experiments.

Therefore, the method is suitable to realize strain patterns/distributions, folding mechanisms and potential fractured domains rather than to predict strain magnitudes and/or mesoscale fracture patterns/orientations within the structure.

On the validation and integration of modelling techniques

All the experiments presented in this work are, in one way or another, based on observations, descriptions and data acquired in the field. Being aware of the advantages and limitations of each modelling technique, a better image of what each model delivers should be obtained, and a feasible explanation of what motivated its use should be given. Validating and integrating the results from different approaches means, hence, gathering the contributions of each modelling tool to construct a unified model of structural evolution, but also involves covering the gaps that each modelling tool leaves, thus complementing each other.

In this sense the analogue models provided new insights at a regional scale, explaining the processes that led to the generation of those initially arcuate, oblique thrusts, which finally ended up in the N-S anticlines of the External Sierras. The modelling was based on field observations of a nearly absent Keuper facies in the core of the N-S anticlines, and reproduced many features of the natural case: larger N-S uplift associated to the emplacement of an E-W foreland-directed thrust in areas with little or no presence of a ductile layer (Keuper facies), larger advance of the deformation front in areas between the transverse structures, N-S anticlines located at the hangingwall of the frontal thrust and plunging towards the hinterland, vertical axis rotation of the hangingwall in the N-S anticlines and wavy (non-straight) morphology of the foreland-directed thrusts (Fig. 11). However, the analogue models neither investigated the internal complexity of the sedimentary cover nor did they study the effect of syn-kinematic sedimentation in the fold growth. Loose sand itself is not a suitable material to model the tight steep structure of the N-S anticlines of the central External Sierras, characterized by a complex interlayering in which the mechanical properties vary along with the stratigraphic sequence (Figs. 2, 13). Instead, the DEM fulfilled this gap and reproduced the structural style of the Pico del Águila anticline after setting up a mechanical stratigraphy that modelled the one described in the field. The different way in which each unit accommodated deformation was replicated by the DEM experiments: pervasive faulting and high internal deformation of the lower units cohabited with gentle folding in the upper units, at the same time that growth strata accommodated a large amount of deformation and equilibrated the anticline against gravitational instabilities (Fig. 14). The internal décollement level (Garumnian facies) acted as a barrier, allowing the upper units to gently fold whereas the lower ones concentrated more deformation by means of fracturing and folding. This gave us new insight into how the stratigraphy of the central External Sierras responded to shortening, and how multiple folding mechanisms acted simultaneously depending on the mechanical properties of each unit. Despite this, the 2D framework of DEM did not give information on other important kinematic features that imply the three-dimensionality (*e.g.*, the clockwise rotation of the N-S anticline, its relationship with the E-W South Pyrenean thrust and associated interference structures) nor the effect of flexural slip, which has been described in the field. This major limitation has been overcome by the 3D reconstruction and geomechanical restoration of the Pico del Águila (mostly based on field "hard" data), which added the third dimension, validated and improved the structural evolution and mechanical response predicted by the analogue and numerical models. The restoration naturally reproduced a vertical-axis rotation of 33º without imposing any kinematic constraint, in such a way that validates the rotation reported by paleomagnetic measurements (Pueyo *et al.*, 2002; Rodríguez-Pintó *et al.*, 2008) and analogue models (Vidal-Royo *et al.*, 2009). It also reported a different evolution of sedimentation and uplift between flanks and a layer-parallel slip as described in the field (Fig. 15). As it was already suggested by the DEM experiments, multiple folding mechanisms were observed acting simultaneously in different units, depending on the mechanical behaviour of each of them. In addition, the restoration pointed out that multiple folding mechanisms acted synchronously also within a given unit, depending on the structural domain of the fold. This combination of folding mechanisms obviously gives rise to a complex distribution of strain through time, in which deformation preferably concentrates in a different structural domain depending on the mechanical properties of each unit (Fig. 16). On the other hand, the limitations and drawbacks of the geomechanical restoration performed in Dynel3D have been mentioned already. The lack of information associated to the limit of the resolution of tetrahedra is partially overcome by the DEM, which reports a different mechanical response by every single unit. The limitations associated to the use of elastic laws to recover large, non-recoverable deformation are overcome by restoring and adding up small increments of deformation, as well as including the effect of faults, décollements and flexural slip. In this way, each volume is required to restore elastically but on the whole, the model experiences finite, permanent strains that are manifested by faulting, décollement and flexural slip offsets (Maerten and Maerten, 2006; Guzofski *et al.*, 2009 who use a similar restoration technique).

In summary, each modelling technique presented in this work tackles new questions on the structural evolution of

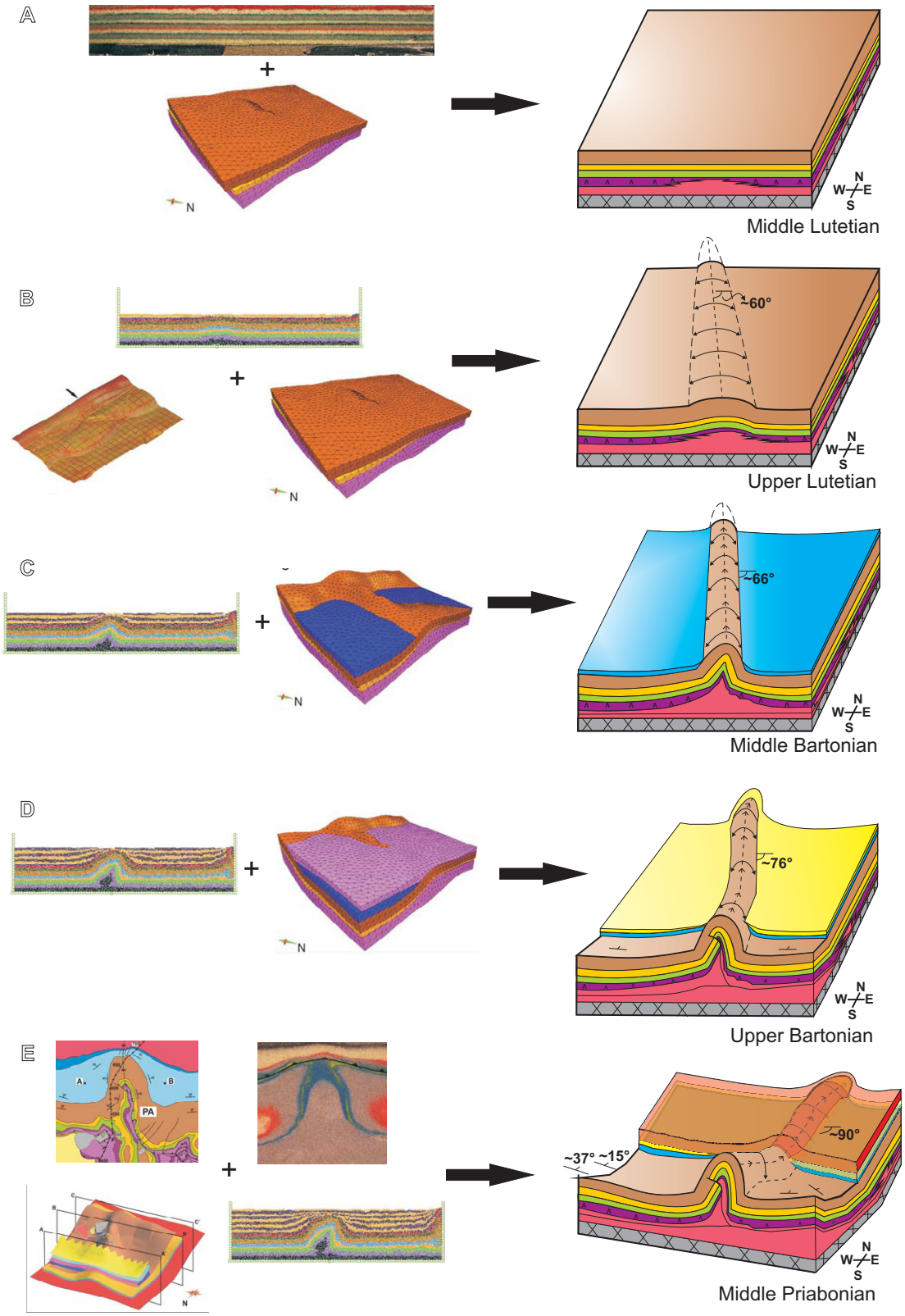

FIGURE 17 | Different sketches summarizing the structural evolution of the Pico del Águila as derived from the presented modelling techniques and the 3D reconstruction of the anticline: A) pre-deformed stage (Middle Lutetian); B) Upper Lutetian, beginning of the deformation; C) Middle Bartonian, deposition of GS-I; D) Upper Bartonian, deposition of GS-II; E) Middle Priabonian, deposition of Campodarbe Fm. (post-kinematic), cease of deformation.

the N-S anticlines of the central External Sierras, provides new insights in accordance to observations in nature, and takes one step further towards the aspects that remained uncovered by other modelling approaches. In other words, the presented modelling techniques contribute with new aspects on the geology of the central External Sierras; validate the results obtained by the other modelling techniques and integrates part of a unified and better constrained geological history of the central External Sierras (Fig. 17).

The Pico del Águila anticline: integrated model of structural evolution

The different modelling results presented in this work combined with the previous studies of the area in many different disciplines allow us to present an integrated model of evolution for the Pico del Águila anticline.

The Pico del Águila is a décollement anticline detached on a complex interplaying of Muschelkalk and Keuper facies (Middle and Upper Triassic). Prior to the deposition of the Cretaceous-Tertiary cover, the area already had a complex structure and a long geological history. According to paleogeographic reconstructions (López-Gómez *et al.*, 2002; Castillo-Herrador, 1974; Jurado, 1990; Salvany, 1990) the region was located in a high of the Triassic extensional basin, in which little sedimentation took place during Upper Triassic times. This structural position influenced the low and irregular stratigraphic thickness of the Keuper facies (red clays and gypsum-bearing clays) observed in the area and the complex interfingering with the pre and syn-extensional Middle Triassic Muschelkalk facies (M2: clays and evaporites, M3: dolomites and dolomitic limestones) (Fig. 17A). In addition, the structural pattern at that time was likely to be complex, and the present-day observed pervasive fracturing partially inherited from Triassic times (Vidal-Royo *et al.*, 2009). This complex structural setting resulted in a mechanically heterogeneous, unevenly distributed Triassic substratum on top of which the Cretaceous-Tertiary sedimentary cover was deposited.

The Pico del Águila anticline started to grow 42.67±0.02Ma ago (Upper Lutetian) (Poblet and Hardy, 1995). Given the mechanical heterogeneities in the Triassic décollement, the anticline was generated at a high angle (between 69º and 57º depending on which value of total rotation is taken) with respect to the E-W regional structural trend (Fig. 17B). The sedimentary cover experienced a larger NNW-SSE uplift in areas with less presence of Keuper facies (lower cover/ductile décollement ratio), at a low angle with the direction of tectonic transport (ca. N-S). These large mechanical contrasts in the basal décollement level also drove the clockwise rotation process, influencing the deformation front to advance at a different velocity depending on the mechanic nature of the décollement at different areas. Given the mechanical complexity of the sedimentary cover, which exhibits a heterogeneous mechanical response, N-S shortening was accommodated by folding instead of generating an oblique thrust ramp, forming an incipient detachment anticline at the same time that carbonatic shallow marine platform sedimentation (Guara DS-3) was being deposited. At ca. 41.52Ma ago a sharp transition from carbonate platform to slope depositional settings took place, beginning the deposition of the glauconite-bearing marls (GS-I of the Arguis Fm.). The deposition of this sequence was characterized by uplift of the anticline, larger than the sedimentation rate. This resulted in a thinning and onlapping of GS-I onto the flanks of the Pico del Águila, which remained uncovered by the sediments of the GS-I (Fig. 17C). This large uplift, the creation of space available for sedimentation, and the transgressive cycle that characterized the deposition of the Guara and Arguis fms. (Millán *et al.*, 1994; Castelltort *et al.*, 2003), controlled the change of sedimentary facies from the Guara shallow marine limestones to the Arguis slope marls. At this time and until ca. 40.04Ma, an increasingly higher sedimentation rate was described. The South Pyrenean thrust front started to generate, adding a slight northwards tilt to the anticline (Fig. 17C). At ca. 40.04Ma there was a change in the depositional environment that led to the end of the deposition of GS-I. Different folding mechanisms characterized the evolution at this early stage: in GS-I kink band migration predominates in the hinge of the associated synclines, and a combination of limb lengthening and limb rotation occurs along the E-W oriented limbs, whereas in the Guara Fm. limb lengthening dominates in the periclinal closure and limb rotation is the main mechanism along the N-S oriented part of the limbs (Fig. 17D). This complex interplay between different folding mechanisms in different units and structural domains characterizes the entire fold growth, and leads to the contrasts in structural style that are described in the field: an internal thrust parallel to the fold trend affects the faulted and complexly deformed Muschelkalk-middle Guara sequence whereas the overlying upper Guara-Campodarbe sequence is more simply folded. With further shortening the emplacement of the South Pyrenean thrust ramp increases the plunge of the anticline at the same time as the progressive rotation takes place (Fig. 17D). At ca. 37.74Ma the depositional setting changed slightly and the presence of benthic foraminifera, bryozoans, bivalves and echinoids is described (Millán *et al.*, 1994). On the whole, the anticline had already rotated ca. 6º at this time from the beginning of deformation. However, as shown by the restoration, flexural slip accentuates the rotation of the upper layers with respect to the lower ones, since a slight additional rotation is observed in the upper units. The anticline, therefore, did not rotate as a rigid block:

the mechanical contrasts in the basal décollement drove the general rotation of the structure as the South Pyrenean thrust advanced, but flexural slip between units allowed additional rotation of each unit as one moves upwards in the stratigraphic sequence. According to Millán *et al.* (1994), after the deposition of GS-III at ca. 37.17Ma the depositional setting changed to a low angle carbonate ramp which consists of marly facies (outer ramp facies) interlayered with carbonate facies (middle ramp facies) rich in benthic pectinids. A significant rotation of ca. 10º was observed with respect to the previous stage as well as an increase of about 4º in the northwards plunge of the anticline. Both increments indicate a larger activity in the emplacement of the South Pyrenean thrust during this period. Deposition of GS-IV (Belsué-Atarés Fm., ca. 36.6Ma), in contrast, did not imply a significant increase in the rotation (barely 2º) and plunge (about 4º) of the anticline. This was the first depositional sequence that covered all the anticline (Fig. 17E), and implied a change in the depositional setting to deltaic lobes prograding on to prodelta marls, made up by coarsening upward sequences of sandstones and thin marly sequences (Millán *et al.*, 1994). Due to the layer parallel slip described in the syn-kinematic rocks, growth sequences accommodated low to moderate strain, with high strain concentrated in the pre-folding sequence, mainly due to the emplacement of the South Pyrenean thrust ramp underneath. Finally, from the top of GS-IV until the cease of deformation (estimated at 34.8±1.72Ma according to Poblet and Hardy, 1995) the depositional setting changed from fluviodeltaic to fluvial environment, characterized by the sandstones, clays and conglomerates of the Campodarbe Fm. The registered rotation was important, of ca. 15º with respect to the previous stage, and an increment in plunge of about 18º (Fig. 17E). This indicates that the emplacement of the South Pyrenean thrust ramp had the most intense activity during this time lapse. The layer-parallel slip led to a differential folding and rotation of the units that generated the asymmetry described in the present-day geometry. Also during this last stage of deformation, normal faulting in the crest of the anticline was described within the entire growth strata, mostly due to outer arc stretching and crestal instabilities.

CONCLUSIONS

Three different modelling techniques have been integrated to better understand the structural evolution of the Pico del Águila anticline (southern Pyrenees, Spain).

Analogue models provide new insights on the evolution of the oblique and transverse structures of the central External Sierras. Based on the uneven distribution of the Triassic detachment level, models simulate the characteristics of the N-S trending anticlines of central External Sierras: synchronous generation with the emplacement of the South-Pyrenean frontal thrust, higher structural relief compared to orogen-parallel structures, absence of a representative ductile décollement in the core, faulting of lower units and folding of upper ones, plunge towards the hinterland, and foreland-side closure not thrusted by the frontal emerging South-Pyrenean thrust.

The Discrete-Element models have been used to test the influence of complex competent/incompetent interlayering and the presence of growth strata in the growth of the Pico del Águila anticline. The mechanical interlayering leads to high shear strain and complex deformation within the incompetent units, whereas the competent units are subject to more distributed shear strain and simple folding. As a result of the different mechanical responses to shortening, it is difficult to explain the evolution of such a structure in terms of simple kinematic models. The addition of growth strata reduces the effects of stretching, extensional faulting and gravitational instabilities on the crest of the anticline. The load of the syn-kinematic package also led the deformation to be more confined in the core of the structure, which is thus tighter than in the absence of growth strata.

The 3D reconstruction and restoration of the Pico del Águila anticline also suggest that the development of a detachment fold in 3D is characterized by a combination of multiple folding mechanisms that occur simultaneously in different units and structural domains during the formation of the anticline. This combination depends on the mechanical properties of the involved materials. Thus, the understanding of fold kinematics should not overlook the mechanical behaviour of the rocks to have a better understanding of the structural evolution.

The proper integration of different modelling techniques deals with the insights that each approach delivers, but also with the limitations of each particular modelling. In this sense, our study presents a model of evolution for the Pico del Águila anticline based on the integration among the analogue, the numerical and the 3D geomechanical restoration modelling of the structure, plus the insights provided by key previous works in the region. Combining multidisciplinary modelling techniques, hence, brings a better understanding of the evolution of this structure as well as the processes that drove the evolution of the N-S detachment anticlines in the External Sierras of the southern Pyrenees.

ACKNOWLEDGMENTS

The authors wish to thank IGEOSS, Paradigm™, and Midland Valley Exploration for providing academic licenses of their

software Dynel3D, Gocad, and Move, respectively. This work is an initiative of the Geomodels Research Institute and the Group of Geodynamics and Basin Analysis (GGAC, 2009 SGR 1198) at the Universitat de Barcelona. Authors acknowledge the work and effort of Dr. Samuel Haines, Dr. Jeffrey Rahl and an anonymous reviewer, who have definitely helped to improve the quality of this article. This research was supported by StatoilHydro and the INTECTOSAL project (CGL2010-21968-CO2-01). O. Vidal-Royo also acknowledges the Agència de Gestió d'Ajuts Universitaris i a la Recerca (AGAUR) for providing a PhD grant (2005 FI 00200) and additional funds (2006 BE-2 00095 and 2008 BE-1 00348) for a 3-month stay at the Hans Ramberg Tectonic Laboratory (Uppsala University, Sweden) and a 3-month stay at the Center for Integrated Petroleum Research (CIPR), and the Department of Petroleum Engineering at The University of Stavanger (UiS) (Norway). We also wish to thank Uppsala University, CIPR and UiS for their logistic support during this period.

REFERENCES

Agterberg, F.P., 1967. Computer techniques in geology. Earth-Science Reviews, 3, 47-77.

Amilibia, A., McClay, K.R., Sàbat, F., Muñoz, J.A., Roca, E., 2005. Analogue Modelling of Inverted Oblique Rift Systems. Geologica Acta, 3(3), 251-271.

Bonini, M., 2003. Detachment folding, fold amplification, and diapirism in thrust wedge experiments. Tectonics, 22(6), 1065, 26pp. doi:10.1029/2002TC001458

Cadell, H.M., 1888. Experimental Researches in mountain building. Royal Society of Edinburgh Transactions, 35, 337-360.

Cagnard, F., Brun, J.P., Gapais, D., 2006. Modes of thickening of analogue weak litospheres. Tectonophysics, 421(1-2), 145-160.

Carmona, A., Clavera, R., Gratacós, O., Hardy, S., 2008. Combining Discrete Element Modelling and process-based models: initial results. Bolletino di Geofisica teorica ed applicata, 49, 358-364.

Castelltort, S., Guillocheau, F., Robin, C., Rouby, D., Nalpas, T., Lafont, F., Echard, R., 2003. Fold control on the stratigraphic record: a quantified sequence stratigraphic study of the Pico del Aguila anticline in the south-western Pyrenees (Spain). Basin Research, 15, 527-551.

Castillo-Herrador, F., 1974. Le Trias évaporitique des basins de la Vallée de l'Ebre et de Cuenca. Bulletin de la Societé Géologique de France, 16, 49-63.

Daudre, A., 1879. Etudes Synthétiques de Géologie Expérimentale, part 1. Dunod (Paris), 828pp.

Fernández, O., 2004. Reconstruction of geological structures in 3D: An Example from the Southern Pyrenees. Doctoral Thesis. Barcelona (Spain), Departament de Geodinàmica i Geofísica, Universitat de Barcelona, 376pp.

Fernández, O., Muñoz, J.A., Arbués. P., Falivene, O., Marzo, M., 2004 . Three-dimensional reconstruction of geological surfaces: An example of growth strata and turbidite systems from the Ainsa basin (Pyrenees, Spain). American Association of Petroleum Geologists Bulletin, 88(8), 1049-1068.

Finch, E., Hardy, S., Gawthorpe, R.L., 2003. Discrete element modelling of contractional fault-propagation folding above rigid basement blocks. Journal of Structural Geology, 25, 515-528.

Finch, E., Hardy, S., Gawthorpe, R.L., 2004. Discrete element modelling of extensional fault-propagation folding above rigid basement fault blocks. Basin Research, 16, 489-506.

Guzofski, C.A., Mueller, J.P., Shaw, J.H., Muron, P., Medwedeff, D.A., Bilotti, F., Rivero, C., 2009. Insights into the mechanisms of fault-related folding provided by volumetric structural restorations using spatially varying mechanical constraints. American Association of Petroleum Geologists Bulletin, 93(4), 479-502.

Hall, J.Sir., 1815. On the vertical position and convolutions of certain strata and their relation with granite. Royal Society of Edinburgh Transactions, 7, 79-108.

Harbaugh, J.W., Merriam, D.F., 1968. Computer applications in stratigraphic analysis. New York (USA), John Wiley Sons Inc., 282pp.

Hardy, S., Finch, E., 2005. Discrete-element modelling of detachment folding. Basin Research, 17, 507-520.

Hardy, S., Finch, E., 2007. Mechanical stratigraphy and the transition from trishear to kink-band fault-propagation fold forms above blind basement thrust faults: A discrete-element study. Marine and Petroleum Geology, 24, 75-90.

Holl, J.E., Anastasio, D.J., 1993. Paleomagnetically derived folding rates, Southern Pyrenees, Spain. Geology, 21(3), 271-274.

Huyghe, D., Mouthereau, F., Castelltort, S., Filleaudeau, P.Y., Emmanuel, L., 2009. Paleogene propagation of the southern Pyrenean thrust wedge revealed by finite strain analysis in frontal thrust sheets: Implications for mountain building. Earth and Planetary Science Letters, 288 (3-4), 421-433.

IGME, 1992. Mapa Geológico de España 1:50000. Hoja 248, Apiés. Madrid, Instituto Geológico y Minero de España, unpublished report, 36pp.

Jurado, M.J., 1990. El Triásico y el Liásico basal evaporíticos del subsuelo de la cuenca del Ebro. In: Ortí, F., Salvany, J.M. (eds.). Formaciones evaporíticas de la Cuenca del Ebro y cadenas periféricas, y de la zona de Levante, Madrid. Enresa, 21-28.

Koyi, H.A., 1997. Analogue modelling: from a qualitative to a quantitative technique–a historical perspective. Journal of Petroleum Geology, 20, 223-238.

Krumbein, W.C., Graybill, F.A., 1965. Application of the general linear model to Map Analysis. An Introduction to Statistical Models in Geology. New York, McGraw-Hill, 319-357.

López-Gómez, K., Arche, A., Pérez-López, A., 2002. Permian and Triassic. In: Gibbons, W., Moreno, T. (eds.). The Geology of Spain. The Geological Society of London, 185-212.

Maerten, L., Maerten, F., 2006. Chronologic modeling of faulted and fractured reservoirs using geomechanically based restoration:

Technique and industry applications. American Association of Petroleum Geologists Bulletin, 90(8), 1201-1226.

Millán, H., Aurell, M., Meléndez, A., 1994. Synchronous detachment folds and coeval sedimentation in the Prepyrenean External Sierras (Spain): a case study for a tectonic origin of sequences and system tracts. Sedimentology, 41(5), 1001-1024.

Millán, H., 1995. Estructura y Cinemática del frente de cabalgamiento surpirenaico en las Sierras Exteriores Aragonesas. Doctoral Thesis. Zaragoza, Departamento de Ciencias de la Tierra, Universidad de Zaragoza, 330pp and Annex.

Nalpas, T., Györfi, I., Guillocheau, F., Lafont, F., Homewood, P., 1999. Influence de la charge sédimentaire sur le développement d'anticlinaux synsédimentaires. Modélisation analogique et exemple du terrain (bordure sud du bassin de Jaca). Bulletin de la Societé Géologique de France, 170(5), 733-740.

Nalpas, T., Gapais, D., Vergés, J., Barrier, L., Gestain, V., Leroux, G., Rouby, D., Kermarrec, J.J., 2003. Effects of rate and nature of synkinematic sedimentation on the growth of compressive structures constrained by analogue models and field examples. In: McCant, T., Saintot, A. (eds.). Tracing Tectonic Deformation Using the Sedimentary Record, London. Geological Society, 208 (Special Publications), 307-319.

Novoa, E., Suppe, J., Shaw, J.H., 2000. Inclined-Shear Restoration of Growth Folds. American Association of Petroleum Geologists Bulletin, 84(6), 787-804.

Oliva-Urcía, B., Pueyo, E.L., 2007. Gradient of shortening and vertical-axis rotations in the Southern Pyrenees (Spain), insights from a synthesis of paleomagnetic data. Revista de la Sociedad Geológica de España, 20 (1-2), 105-118.

Place, D., Mora, P., 2001. A random lattice solid model for simulation of fault zone dynamics and fracture processes. In: Mulhaus, H.B., Dyskin, A.V., Pasternak, E. (eds.). Bifurcation and Localisation Theory for Soils and Rocks '99. Rotterdam/ Brookfield, A.A. Balkema, 321-332.

Poblet, J., Hardy, S., 1995. Reverse modelling of detachment folds, application to the Pico del Aguila anticline in the South Central Pyrenees (Spain). Journal of Structural Geology, 17, 1707-1724.

Poblet, J., McClay, K.R., Storti, F., Muñoz, J.A., 1997. Geometries of syntectonic sediments associated with single-layer detachment folds. Journal of Structural Geology, 19(3-4), 369-381.

Pueyo, E.L., Millán, H., Pocoví, A., 2002. Rotation velocity of a thrust: a paleomagnetic study in the External Sierras (Southern Pyrenees). Sedimentary Geology, 146(1), 191-208.

Puigdefàbregas, C., 1975. La Sedimentación Molásica en la Cuenca de Jaca. Monografías del Instituto de Estudios Pirenaicos. Instituto de Estudios Pirenaicos, Jaca. Número, 104, 153pp and Annexes.

Rodríguez-Pintó, A., Pueyo, E.L., Pocoví, A., Barnolas, A., 2008. Cronología de la actividad rotacional en el sector central del frente de cabalgamiento de Sierras Exteriores (Pirineo Occidental). Geotemas, 10, 1207-1210.

Salvany, J.M., 1990. Introducción a las evaporitas triásicas de las cadenas periféricas de la cuenca del Ebro: Catalánides, Pirineo y Región Cantábrica. In: Ortí, F., Salvany, J.M. (eds.). Formaciones evaporíticas de la Cuenca del Ebro y cadenas periféricas, y de la zona de Levante, Madrid. Enresa, 21-28.

Soler, M., Puigdefàbregas, C., 1970. Líneas generales de la geología del Alto Aragón Occidental. Pirineos, 96, 5-20.

Teixell, A., García-Sansegundo, J., 1995. Estructura del sector central de la Cuenca de Jaca (Pirineos Meridionales). Revista de la Sociedad Geológica de España, 8(3), 215-228.

Vidal-Royo, O., Koyi, H.A., Muñoz, J.A., 2009. Formation of orogen-perpendicular thrusts due to mechanical constrasts in the basal décollement in the Central External Sierras (Southern Pyrenees, Spain). Journal of Structural Geology, 31, 523-539.

Vidal-Royo, O., Hardy, S., Muñoz, J.A., 2011a. The roles of complex mechanical stratigraphy and syn-kinematic sedimentation in fold development: Insights from discrete-element modelling and application to the Pico del Águila anticline (External Sierras, Southern Pyrenees). In: Poblet, J., Lisle, R.J. (eds.). Kinematic Evolution and Structural Styles of Fold-and-Thrust Belts. Geological Society, 349 (Special Publications), 45-60.

Vidal-Royo, O., Cardozo, N., Muñoz, J.A., Hardy, S., Maerten, L., 2011b. Multiple mechanisms driving detachment folding as deduced from 3D reconstruction and geomechanical restoration: The Pico del Águila anticline (External Sierras, Southern Pyrenees). Basin Research, 23, 1-19. doi: 10.1111/j.1365-2117.2011.00525.x

Weijermars, R., 1986. Flow behaviour and physical chemistry of bouncing putties and related polymers in view of tectonic laboratory applications. Tectonophysics, 124, 325-358.

Manuscript received April 2010;
revision accepted December 2011;
published Online May 2012